QR Decomposition-based Cyclic Prefixed Single-Carrier Transmissions for Cooperative Communications: Concepts and Research Landscape

Article *in* IEEE Communications Surveys & Tutorials · July 2022

DOI: 10.1109/COMST.2022.3194997

6 authors, including:

Kyeong Jin Kim
Mitsubishi Electric Research Laboratories
246 PUBLICATIONS **3,064** CITATIONS

SEE PROFILE

Hongwu Liu
Shandong Jiaotong University
113 PUBLICATIONS **713** CITATIONS

SEE PROFILE

Miaowen Wen
South China University of Technology
349 PUBLICATIONS **7,884** CITATIONS

SEE PROFILE

Theodoros Tsiftsis
University of Thessaly
337 PUBLICATIONS **9,619** CITATIONS

SEE PROFILE

QR Decomposition-based Cyclic Prefixed Single-Carrier Transmissions for Cooperative Communications: Concepts and Research Landscape

Kyeong Jin Kim, Hongwu Liu, Miaowen Wen, Theodoros A. Tsiftsis,
Philip V. Orlik, and H. Vincent Poor

Abstract

As an alternative transmission scheme to orthogonal frequency division multiplexing (OFDM), cyclic prefixed single- carrier (CP-SC) transmissions have been widely adopted to overcome the shortcomings of OFDM. How to exploit the achievable full diversity in frequency selective fading channels is the key question in applying CP-SC-based transmissions. Thus, in this tutorial, we focus on recent research in the areas related to CP-SC transmissions for cooperative wireless systems. After explaining the basic concept and operation of CP-SC transmissions, we introduce various types of diversity that are achievable by CP-SC transmissions. To achieve various types of diversity, it is necessary to employ the QR decomposition (QRD)-M-based data detection in the receiver. To verify the benefits of CP-SC transmissions in terms of diversity gain, we exemplify various wireless systems for relaying, spectrum sharing, physical layer security, and distributed cyclic delay diversity, and provide link-level simulations. Especially, as alternative metrics of reliability, which is one of the key features of 5G and beyond 5G (B5G) systems, we evaluate the average symbol error rate and outage probability. Finally, we discuss potential research directions with CP-SC transmissions in emerging systems.

Index Terms

Cyclic prefixed single-carrier transmissions, QR decomposition, cooperative communications, full diversity, spectrum sharing, physical layer security, and distributed cyclic delay diversity.

Kyeong Jin Kim and Philip V. Orlik are with Mitsubishi Electric Research Laboratories (MERL), Cambridge, MA 02139 USA (e-mail: kkim@merl.com).

Hongwu Liu is with Shandong Jiaotong University, Jinan 250357, China (e-mail: liuhongwu@sdjtu.edu.cn).

Miaowen Wen is with the South China University of Technology, Guangzhou 510641, China (e-mail: eemwwen@scut.edu.cn).

Theodoros A. Tsiftsis is with the School of Intelligent Systems Science and Engineering, Jinan University, Zhuhai 519070, China (e-mail: theo_tsiftsis@jnu.edu.cn).

H. Vincent Poor is with the Department of Electrical and Computer Engineering, Princeton University, Princeton, NJ 08544 USA (e-mail: poor@princeton.edu).

I. INTRODUCTION

As the data rate increases, a wireless communication channel tends to exhibit more multipath components, so that it becomes frequency selective. Since the signal energy associated with each symbol is spread out in time, inter-symbol interference (ISI) will be caused between adjacent transmitted symbols. Thus, in realistic environments, how to handle ISI becomes a challenging problem. Orthogonal frequency division multiplexing (OFDM) is one solution to this problem, and it is used in many applications, including 4G and 5G mobile networks, digital video-second generation terrestrial/digital audio broadcasting (DVB-T2/DAB) [1], [2], multimedia data streaming, gaming, mmWave wireless personal area network (WPAN) [3], wireless local area networks (WLANs) [4]–[7], and power line communications (PLC) [8]. Many of these wireless applications are specified by IEEE 802.11n [4], IEEE 802.11ac [5], IEEE 802.11ad [6], IEEE 802.11ay [7], and IEEE Std 1901-2010 [8]. Particularly, to support other applications, such as augmented reality (AR) and virtual reality (VR) that require greater throughput and reliability with lower latency, IEEE 802.11ay is under standardization. These applications are one of the key usages of 5G and B5G to increase worker's safety and security in the industrial domain. Furthermore, IEEE Std 1901-2010 specifies a broadband PLC technology for smart energy, smart grid, Internet of Things (IoT), industrial IoT (IIoT), and vehicular transportation platforms, which are also related to the use cases of 5G and B5G.

Making the symbol rate of OFDM subcarriers relatively lower and the symbol period relatively longer, and combining with the cyclic prefix (CP), OFDM can reduce ISI caused by a time-dispersive channel. Thus, these existing systems and mentioned standards enjoy the benefits from OFDM transmissions in the presence frequency selective fading. However, owing to the following inherent impairments, the cyclic prefixed single-carrier (CP-SC) transmission has been adopted in various wireless systems as an alternative transmission technique:

- Due to the use of a large number of independently modulated subcarriers for transmissions, OFDM has the possibility of causing a high peak-to-average power ratio (PAPR). For satellite communications, SC-OFDM, which is a discrete Fourier transform (DFT)-precoded OFDM with the CP, was proposed to reduce PAPR and make OFDM less sensitive to phase noise [9]. A high PAPR can be caused by a random addition of subcarriers in the time domain (TD). In particular, when the peak amplitudes of the different signals are aligned in phase at the same time, high peaks occur [10]. The PAPR determines a dynamic range of the digital-to-analog converter (DAC) and the analog-to-digital converter (ADC) [11]. Thus, OFDM can make the system sensitive to nonlinearities, and it causes a large backoff from the full scale output, which lowers the efficiency of the power amplifiers (PAs). PAs are one of the critical building blocks that determine several important metrics such as the energy efficiency and reliability of wireless systems [12]. In contrast to OFDM, a much lower PAPR can be expected with CP-SC, so that CP-SC-based systems can ease the demand for high efficiency PAs and dynamic range of DAC and ADC. In particular, for SC and OFDM, the PAPR is listed in Table I with a mmWave waveform over various modulations [12]. Taking advantage of a lower PAPR, CP-SC has been used

at the terminal side in uplink communications of 3GPP Long Term Evolution (LTE) [13]. In particular, for some types of distributed nodes that mainly conduct uplink communications with the controller, battery life can be extended by reducing the high PAPR.

TABLE I

PAPR WITH FILTER ROLL-OFF FACTOR=0.25 [12]

SC-QPSK	SC-16QAM	SC-64QAM	OFDM-QPSK	OFDM-16QAM	OFDM-64QAM
5 dB	6.9 dB	7.1 dB	9.7 dB	10.4 dB	11 dB

- High sensitivity to inter-carrier interference (ICI) caused by carrier frequency offsets (CFOs). If CFOs are not compensated effectively, a significant performance degradation is expected in OFDM-based systems such as high-speed optical communication systems [14] and ultra-wideband (UWB) systems [15]. For underwater acoustic communications in the presence of a relatively high Doppler shift, it is difficult to achieve orthogonality between subcarriers [16], which is the key requirement of OFDM. In addition, OFDM may not work effectively for PLC [17], where the channels are more hostile due to fast time variation and the existence of high amplitude impulse noise. Since CFO does not cause ICI for CP-SC transmissions, CP-SC transmissions do not require computationally demanding CFO compensation algorithms.
- OFDM is sensitive to spectral nulls due to receiver processing in the frequency domain [18]. To overcome this weakness, it is necessary to employ forward error correction (FEC) coding [19] to exploit frequency diversity. In contrast to OFDM, CP-SC can achieve frequency diversity in frequency selective channels without employing a strong FEC code [20].
- Since the packet length may not be adjusted dynamically [21] by OFDM, OFDM is less adoptable to burst transmissions. In contrast, CP-SC is flexible in dealing with the need for various burst transmissions. Thus, it is suitable for 5G and B5G networks, sensor networks, and IoT and IIoT networks that have increasingly stringent performance requirements of throughput, latency, reliability, availability, security, and device density, where transmitted data may consist of short messages, such as machine control orders, sensor information, and health care data, which consist of only a few bytes, while requiring to be transmitted periodically and frequently. Thus, comparing with OFDM, CP-SC is more appropriate in environments composed of heterogeneous sensors and devices such as static, mobile, and ad-hoc devices. In particular, CP-SC makes possible simple signal processing that composes a symbol block and appends CP in the transmitter, so that a cost effective distributed system can be feasible. This advantage has led to the development of a new power efficient transmit diversity scheme, called the distributed cyclic delay diversity (dCDD) for CP-SC transmissions [22].

The motivation and contribution of this paper are summarized as follows:

- To help the readers understand CP-SC transmissions, we introduce its concept and fundamental operation.
- To help the readers understand how to achieve the full diversity, we introduce QRD-M-based data detection that exploits the advantages of CP-SC transmissions in the time dispersive channel environment. We also introduce how to achieve multiuser diversity by employing opportunistic user scheduling.
- To help the readers see how CP-SC transmissions have been applied to cooperative systems, we exemplify the wireless systems for relaying [23]–[26], spectrum sharing [27]–[30], physical layer security (PLS) [31]–[33], and transmit diversity [29], [34], [35]. These systems are composed by distributed devices/nodes enabling cooperation among them, so that they are related to emerging 5G wireless systems.
- To help the readers see how much performance can be improved for the above exemplified systems, we provide analysis based on the simulations.

A. Summary of the Existing Works

- Relaying systems: The principal objective of the papers [23]–[26] is to increase reliability of CP-SC transmissions to extend the operating regions, and increase the link quality and throughput of distributed communication systems.
- Spectrum sharing systems: To increase capability of the secondary user (SU) to access licensed spectrum assigned to the primary user (PU), [27]–[30] have proposed multiple diversity schemes within the distributed system.
- PLS systems: By effectively exploiting the characteristics of wireless channels, PLS has the capability to secure data transmissions over wireless distributed networks. The primary objective of CP-SC transmissions [31]–[33] is to exploit full diversity in frequency-selective fading channels.
- dCDD-based transmit diversity systems: Among the above-mentioned benefits of CP-SC transmissions, simple transmitter operation, ease of achieving multipath diversity and spatial diversity, and ease of time and frequency synchronization among distributed nodes, are primary considerations in the deployment of dCDD for various distributed systems such as spectrum sharing systems [29], relaying systems [34], and PLS systems [35].

B. Organization

In Section II, the basic concept of the CP-SC transmission is provided, and variants of CP-SC transmissions, including training-aided SC (TA-SC), and zero-padded SC (ZP-SC) are introduced. Additional explanations and interpretations of QRD-M-based data detection, how to achieve multipath diversity, opportunistic user scheduling to achieve multiuser diversity, and dCDD-based transmit diversity are also introduced. In Section III, we exemplify CP-SC based relaying systems in Section III-A, spectrum sharing systems in Section III-B, PLS systems in Section III-C, and dCDD-based systems in Section III-D. Future directions are considered in Section IV. Finally, conclusions

are discussed in Section V. To show how three different types of diversity are identified among exemplified systems, we provide Fig. 1. Abbreviations and mathematical notations used in this paper are summarized in Table II and Table III, respectively.

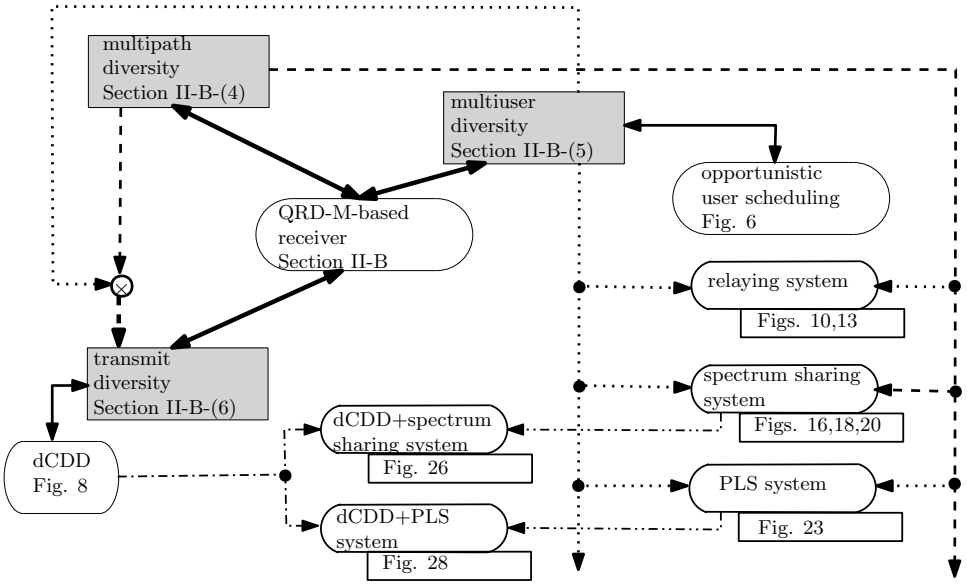

Fig. 1. The overall structure of the paper.

C. Scope and Assumptions

- We mainly focus on base-band processing for communications under an assumption that channel state information (CSI) is known to the system. Furthermore, we only consider a time dispersive channel, which is closer to the realistic channel environment.
- We do not consider the large scale fading, which is related to the distance between two devices/nodes to simplify mathematical expressions for the signal-to-noise ratio (SNR), signal-to-interference-and-noise ratio (SINR), signal-to-interference ratio (SIR), and performance analysis.
- We assume that tight time and frequency synchronization is achieved among distributed devices/nodes. To support this assumption, 802.11AS [36], [37], a subset of IEEE 1588 [36], is used between the grand-master clock and the endpoint clock [36], [37]. For a full distributed system, according to the best master clock algorithm, one device or node is selected as a grand-master clock provider to form the synchronization hierarchy structure.
- We assume that the noise power realized by the receiving channel of the receiver (Rx) is given by σ_z^2.
- We use the average symbol error rate (ASER), denoted by P_e, outage probability, and secrecy outage probability as performance metrics. For a realized SNR, γ, the outage probability at a given SNR threshold, $\gamma_{\text{th}} = 1$ dB, is

defined by $P_{\text{OP}}(\gamma_{\text{th}}) = \Pr(\gamma < \gamma_{\text{th}})$. The transmission capacity by legitimate transmissions and the interceptable capacity by the illegitimate user are given by $C_L = \log_2(1+\gamma_L)$ and $C_E = \log_2(1+\gamma_E)$, respectively. With γ_L and γ_E respectively denoting realized SNRs by legitimate transmissions and intercepted transmissions, the secrecy capacity is given by $C_s = [C_L - C_E]^+$, where $[x]^+ \triangleq \max(0, x)$. For a given rate $R_s = 1$, the secrecy outage probability (SOP) is given by $P_{\text{SOP}}(R_s) = \Pr(C_s < R_s)$. In addition to these metrics, for secrecy capacity C_s, the probability of non-zero achievable secrecy rate is given by $\Pr(C_s > 0)$.

- We define the diversity gain as the slope measured from the ASER, that is, $-\log_{10}(\text{ASER})$ in terms of $\log_{10}(\text{operating SNR})$. Similarly, the diversity gain can be obtained from the outage probability.

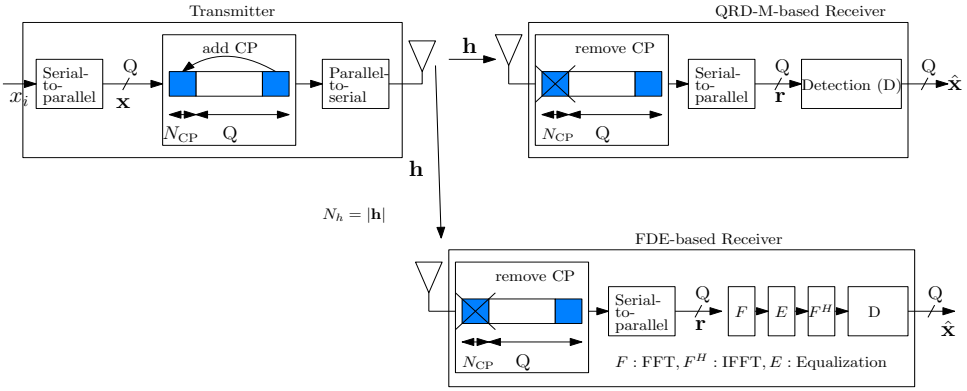

Fig. 2. Block diagram of the wireless communication system employing CP-SC transmissions. QR decomposition-M (QRD-M)-based and frequency domain equalizer (FDE)-based data detectors are respectively considered in two receivers.

II. Basic Concept of CP-SC Transmissions and Diversity

Fig. 2 illustrates a block diagram of a typical wireless communication system that employs CP-SC transmissions. Having applied serial-to-parallel operation to the input modulated symbol stream, $\{x_i\} \in \mathbb{C}$, we first obtain the transmission block symbol composed by Q modulated symbols, $\boldsymbol{x} \in \mathbb{C}^{Q\times 1}$, which satisfies $E\{\boldsymbol{x}\} = \mathbf{0}$ and $E\{\boldsymbol{x}\boldsymbol{x}^H\} = \boldsymbol{I}_Q$. A CP composed of N_{CP} modulated symbols is prefixed to the front of $\boldsymbol{x}$ to prevent inter-block symbol interference (IBSI) and ISI. Note that when Q and N_{CP} are determined beforehand, the CP addition can be accomplished as an input operation of the serial-to-parallel converter. In general, in low latency communications, how to reduce the size of the CP will be an open problem to minimize the spectral efficiency and energy efficiency losses [38] while combating multipath fading. After applying parallel-to-serial operation, the modulated symbols are propagated through a channel, $\boldsymbol{h}$, which is assumed to be composed of N_h multipath components to represent frequency selectivity, that is, $\boldsymbol{h} = [h_0, \ldots, h_{N_h-1}]^T \in \mathbb{C}^{N_h\times 1}$. According to the adopted channel characteristics, it is required that $N_{\text{CP}} \geq N_h$.

TABLE II

ABBREVIATIONS

ADC	analog-to-digital converter	AF	amplify-and-forward
AN	artificial noise	AR	augmented reality
ASER	average symbol error rate	B5G	beyond 5G
BRS	best relay selection	BS	base station
BTS	best terminal selection	CDD	cyclic delay diversity
CFO	carrier frequency offset	CoMP	coordinated multi-point
CP	cyclic prefix	CP-SC	cyclic-prefixed single carrier
CR	cognitive radio	CSI	channel state information
CU	control unit	DAB	digital audio broadcasting
DAC	digital-to-analog converter	dCDD	distributed cyclic delay diversity
DF	decode-and-forward	DFT	discrete Fourier transform
DSA	dynamic spectrum aggregation	DU	distributed unit
DVB-T2	digital video broadcasting-second generation terrestrial	EU	eavesdropping user
FDE	frequency domain equalizer	FEC	forward error correction
gNB	gNodeB	IBSI	inter-block symbol interference
ICI	inter-carrier interference	IDFT	inverse DFT
IIoT	industrial internet of things	IMGF	inverse moment generating function
IoT	internet of things	ISI	inter-symbol interference
LTE	long term evolution	LU	legitimate user
MGF	moment generating function	MIMO	multiple-input multiple-output
MISO	multiple-input single-output	MLD	maximum likelihood detector
MMSE	minimum mean-square error	MPSK	M-ary phase-shift keying
MRC	maximal-ratio combining	NOMA	non-orthogonal multiple access
OFDM	orthogonal frequency division multiplexing	PA	power amplifier
PDF	probability density function	PAPR	peak instantaneous power to average power ratio
PBRS	partial best relay selection	PLC	power line communications
PLS	physical layer security	PU	primary user
QRD	QR decomposition	QRD-M	QR decomposition-M
RF	radio frequency	RRH	remote radio head
RX	receiver	SC	single carrier
SC-FDE	single carrier-frequency domain equalizer	SeC	selection combining
SIMO	single-input multiple-output	SINR	signal-to-interference-and-noise ratio

SISO	single-input single-output	SNR	signal-to-noise ratio
SU	secondary user	TAS	transmit antenna selection
TA	training-aided	TA-SC	training-aided SC
TD	time domain	TSN	time sensitive networking
TVWS	TV white space	UW	unique word
UWB	ultra-wideband	VR	virtual reality
WLAN	wireless local area network	WPAN	wireless personal area network
ZP	zero-padded	ZP-SC	zero-padded SC

TABLE III

MATHEMATICAL NOTATION

Notation	Description
$\mathbf{0}$	All zero vector or matrix
P_e	Average symbol error rate
$\mathcal{CN}(m, C)$	Complex Gaussian distribution with mean m and covariance C
$diag(\boldsymbol{a})$	Diagonal matrix determined by vector $\boldsymbol{a}$
$E\{\cdot\}$	Expectation
$\lfloor \cdot \rfloor$	Floor function
$\boldsymbol{I}_Q$	$Q \times Q$ identity matrix
$\|\boldsymbol{a}\|^2$	L_2 norm defined by $\boldsymbol{a}^H \boldsymbol{a}$
$\boldsymbol{A}, [\boldsymbol{A}]_{i,j}$	Matrix $\boldsymbol{A}$ with (i, j)th element
$\Pr(C_s > 0)$	Non-zero secrecy rate
$P_{\text{OP}}(\gamma_{\text{th}})$	Outage probability at outage threshold γ_{th}
γ	Realized SNR at the receiver
C_s	Secrecy capacity
$P_{\text{SOP}}(R_s)$	Secrecy oitage probability at a rate R_s
$\mathbb{C}$	The set of complex numbers
C_L	Transmission capacity by legitimate transmissions
$(\cdot)^T, (\cdot)^H$	Transpose and conjugate transpose
$\boldsymbol{a}, \|\boldsymbol{a}\|, [\boldsymbol{a}]_j$	Vector $\boldsymbol{a}$ with its size $\|\boldsymbol{a}\|$ and ith element of $\boldsymbol{a}$
$\boldsymbol{b} = [\boldsymbol{a}]_{(1:Q,1)}$	Vector $\boldsymbol{b}$, composed by the first Q elements of vector $\boldsymbol{a}$
$\boldsymbol{a}_{(i)}$	ith ordered vector determined by the magnitude, $\|\boldsymbol{a}\|^2$

When the receiver removes the CP-related signal first, the received signal, $\boldsymbol{r} \in \mathbb{C}^{Q\times 1}$, is expressed as follows:

$$\boldsymbol{r} = \sqrt{P_T}\boldsymbol{H}_{\mathrm{CPSC}}\boldsymbol{x} + \boldsymbol{z} \tag{1}$$

where P_T denotes the transmission power. The additive noise over all the channels is given by $\boldsymbol{z} \sim \mathcal{CN}(\boldsymbol{0}, \sigma_z^2\boldsymbol{I}_Q)$. Due to the use of the CP, a discrete time linear convolution is converted into a discrete time circular convolution. Thus, an equivalent channel channel matrix, $\boldsymbol{H}_{\mathrm{CPSC}} \in \mathbb{C}^{Q\times Q}$, becomes a right circulant matrix [20], [39], whose every row vector is the same as the previous row vector with a shift to the right by one. Thus, every row vector has the same vector norm. From (1), all the SC transmissions require the system to use block-wise receiver operation, which is different from OFDM that applies a data symbol detection for each subcarrier. For OFDM, the channel bandwidth is divided by a fixed number of subcarriers and a baseband symbol is modulated onto a narrowband subcarrier. In contrast, for CP-SC, $\boldsymbol{x}$ is represented by a baseband pulse that occupies the entire bandwidth of the channel and is modulated to a single passband carrier [40].

- When we assume $Q = 6$, $\boldsymbol{h} = [h_0, h_1, h_2]^T$, and $N_{\mathrm{CP}} = 3$, then $\boldsymbol{H}_{\mathrm{CPSC}}$ is given by

$$\boldsymbol{H}_{\mathrm{CPSC}} = \begin{bmatrix} h_0 & 0 & 0 & 0 & h_2 & h_1 \\ h_1 & h_0 & 0 & 0 & 0 & h_2 \\ h_2 & h_1 & h_0 & 0 & 0 & 0 \\ 0 & h_2 & h_1 & h_0 & 0 & 0 \\ 0 & 0 & h_2 & h_1 & h_0 & 0 \\ 0 & 0 & 0 & h_2 & h_1 & h_0 \end{bmatrix} \tag{2}$$

  so that the right circulant matrix, $\boldsymbol{H}_{\mathrm{CPSC}}$, is completely specified by its first column vector, $[\boldsymbol{h}^T, \boldsymbol{0}_{1\times Q-|\boldsymbol{h}|}]^T \in \mathbb{C}^{Q\times 1}$ [41]. Based on the property that a right circulant matrix, $\boldsymbol{A}$, is decomposed as $\boldsymbol{A} = \boldsymbol{F}^H\boldsymbol{\Omega}\boldsymbol{F}$, where $\boldsymbol{F}$ is the DFT matrix and $\boldsymbol{\Omega}$ is a diagonal matrix with its eigenvalues given by $\boldsymbol{\Omega} = diag(\boldsymbol{F}[\boldsymbol{h}^T, \boldsymbol{0}_{1(\times Q-|\boldsymbol{h}|)}]^T)$. Thus, a circulant matrix is diagonalized by the DFT matrix [41].

Depending on the further objective in addition to the objective of appending the CP, namely removing ISI caused by the time dispersive channel, different types of the CP such as the training-aided (TA) prefix [6], [42] and zero-padded (ZP) prefix [43] have been proposed. Thus, we introduce their respective impact on the received signals with SC transmissions and performance comparison with respect to CP-SC transmissions in the sequel.

A. TA-SC and ZP-SC Transmissions

1) TA-SC transmissions: In contrast to CP-SC transmissions, TA-SC transmissions append a unique word (UW) or training sequence, for example, Golay complementary sequences [6] and Zadoff-Chu sequences [44]. That is, an aggregated transmission block symbol is given by $\boldsymbol{x}_{\mathrm{TA}} = [\boldsymbol{x}^T, \boldsymbol{t}_{\mathrm{UW}}^T]^T \in \mathbb{C}^{(Q+N_{\mathrm{UW}})\times 1}$, where $\boldsymbol{t}_{\mathrm{UW}}$ denotes the UW with $N_{\mathrm{UW}} = |\boldsymbol{t}_{\mathrm{UW}}|$. Since $\boldsymbol{t}_{\mathrm{UW}}$, appended in the current transmission block symbol, is identical to the last sub-block of the previous transmission block symbol, $\boldsymbol{t}_{\mathrm{UW}}$ works as the CP in the current transmission block symbol.

Thus, ISI can be removed as CP-SC transmissions with the condition of $N_{\rm UW} \geq N_h$. Owing to this uniqueness, the primary usage of the UW is the channel estimation [6], [45]. In contrast to CP-SC transmissions, the actual transmission block symbol can be recognized as $\tilde{\boldsymbol{x}}_{\rm TA} = [\boldsymbol{t}_{\rm UW}^T, \boldsymbol{x}_{\rm TA}^T]^T$, so that the received signal, after removing the UW related signal part, $\boldsymbol{r}_{\rm TA} \in \mathbb{C}^{(Q+N_{\rm UW})\times 1}$, is expressed as follows:

$$\boldsymbol{r}_{\rm TA} = \sqrt{P_T}\boldsymbol{H}_{\rm TA}\boldsymbol{x}_{\rm TA} + \boldsymbol{z}_{\rm TA} \tag{3}$$

where $\boldsymbol{H}_{\rm TA} \in \mathbb{C}^{(Q+N_{\rm UW})\times(Q+N_{\rm UW})}$ becomes the right circulant matrix as that of the CP-SC transmission. Thus, $\boldsymbol{H}_{\rm TA}$ is specified by its first column vector, $[\boldsymbol{h}^T, \boldsymbol{0}_{1\times(Q-|\boldsymbol{h}|+N_{\rm UW})}]^T$. The additive noise over all the channels is denoted by $\boldsymbol{z}_{\rm TA} \sim \mathcal{CN}(\boldsymbol{0}, \sigma_z^2\boldsymbol{I}_{(Q+N_{\rm UW})})$.

2) ZP-SC transmissions: In ZP-SC transmissions, an aggregated transmission block symbol is processed by $\boldsymbol{x}_{\rm ZP} = [\boldsymbol{x}^T, \boldsymbol{0}_{\rm ZP}^T]^T \in \mathbb{C}^{(Q+N_{\rm ZP})\times 1}$, so that the received signal is given by

$$\boldsymbol{r}_{\rm ZP} = \sqrt{P_T}\boldsymbol{H}_{\rm ZP}\boldsymbol{x} + \boldsymbol{z}_{\rm ZP} \tag{4}$$

where $\boldsymbol{H}_{\rm ZP} \in \mathbb{C}^{(Q+N_{\rm UW})\times(Q)}$ becomes the non-symmetric Toeplitz matrix specified by its first column vector, $[\boldsymbol{h}^T, \boldsymbol{0}_{1\times(Q-|\boldsymbol{h}|+N_{\rm ZP})}]^T$, and first row vector, $[h_0, \boldsymbol{0}_{1\times Q-1}]$. Thus, by using the appended zeros, ISI can be removed when $N_{\rm ZP} \geq N_h$. The additive noise over all the channels is denoted by $\boldsymbol{z}_{\rm ZP} \sim \mathcal{CN}(\boldsymbol{0}, \sigma_z^2\boldsymbol{I}_{(Q+N_{\rm ZP})})$. In particular, a zero padding provides a guard time for RF beam switching and noise plus interference estimation. Furthermore, it enables processing for high Doppler shifts compensation [43].

B. QRD-M-based Data Detection

Without loss of generality, let us mainly consider CP-SC transmissions. The maximum likelihood (ML) data detection of $\boldsymbol{x}$ can be made by

$$\hat{\boldsymbol{x}}_{\rm ML} = \arg\min_{\boldsymbol{x}\in|\boldsymbol{x}|^Q} \|\boldsymbol{y} - \sqrt{P_T}\boldsymbol{H}_{\rm CPSC}\boldsymbol{x}\|^2. \tag{5}$$

When we apply the QR decomposition (QRD) to the channel matrix, $\boldsymbol{H}_{\rm CPSC}$, then it is decomposed by $\boldsymbol{H}_{\rm CPSC} = \boldsymbol{Q}\boldsymbol{R}$, where $\boldsymbol{Q}$ and $\boldsymbol{R}$ are respectively the unitary matrix and upper triangular matrix [46]. Since the ML cost does not change by multiplying it by the unitary matrix, $\boldsymbol{Q}^H$, we can evaluate (5) as follows:

$$\hat{\boldsymbol{x}}_{\rm ML} = \arg\min_{\boldsymbol{x}\in|\boldsymbol{x}|^Q} \|\tilde{\boldsymbol{y}} - \sqrt{P_T}\boldsymbol{R}\boldsymbol{x}\|^2 \tag{6}$$

where $\tilde{\boldsymbol{y}} = \boldsymbol{Q}^H\boldsymbol{y}$ and $\boldsymbol{R} = \boldsymbol{Q}^H\boldsymbol{H}_{\rm CPSC}$.

Now using the property of $\boldsymbol{R}$, (5) can be written as (7), which is provided at the top of the next page. In addition, $\mu_q \triangleq \{[\boldsymbol{x}]_q, [\boldsymbol{x}]_{q+1}, \ldots, [\boldsymbol{x}]_Q\}$ and the cost $m_q([\tilde{\boldsymbol{y}}]_q; \mu_q) = \|[\tilde{\boldsymbol{y}}]_q - \sqrt{P_T}[\boldsymbol{R}]_{q,q}[\boldsymbol{x}]_q - \sqrt{P_T}\sum_{l=q+1}^{Q}[\boldsymbol{R}]_{q,l}[\boldsymbol{x}]_l\|^2$. To obtain a feasible solution from this minimization, the breadth-first tree-search based M-algorithm is utilized in

$$\hat{\boldsymbol{x}}_{\mathrm{ML}} = \arg \min_{\boldsymbol{x}\in|\boldsymbol{x}|^Q} \Big(([\tilde{\boldsymbol{y}}]_Q - \sqrt{P_T}[\boldsymbol{R}]_{Q,Q}[\boldsymbol{x}]_Q)^2 + ([\tilde{\boldsymbol{y}}]_{Q-1} - \sqrt{P_T}[\boldsymbol{R}]_{Q-1,Q-1}[\boldsymbol{x}]_{Q-1} - \sqrt{P_T}[\boldsymbol{R}]_{Q-1,Q}[\boldsymbol{x}]_Q)^2 + \ldots$$
$$+([\tilde{\boldsymbol{y}}]_1 - \sqrt{P_T}[\boldsymbol{R}]_{1,1}[\boldsymbol{x}]_1 - \sqrt{P_T}[\boldsymbol{R}]_{1,2}[\boldsymbol{x}]_2 - \sqrt{P_T}\sum\nolimits_{j=3}^{Q}[\boldsymbol{R}]_{1,j}[\boldsymbol{x}]_j)^2 \Big)$$
$$= \arg \min_{\boldsymbol{x}\in|\boldsymbol{x}|^Q} \sum\nolimits_{q=1}^{Q} m_q([\tilde{\boldsymbol{y}}]_q; \mu_q) \tag{7}$$

such a way that at the detection stage, q, we first compute $M_{\text{QRD-M}}C$ accumulated costs for signal constellation size C, and then keep only $M_{\text{QRD-M}}$ accumulated costs for the next detection stage, $q-1$. Thus, it is called the QRD-M-based data detection algorithm.

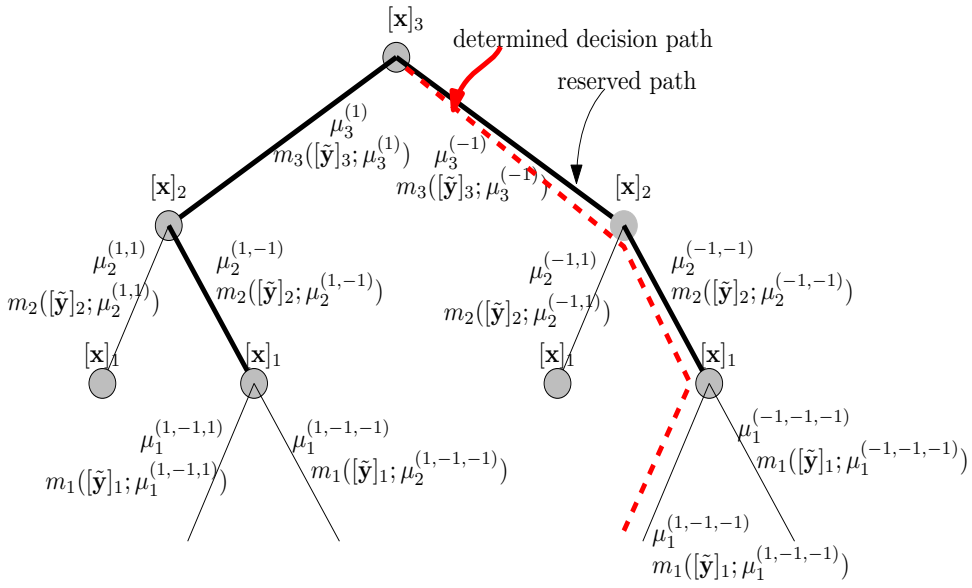

Fig. 3. One example of QRD-M-based data detection process.

Referring to Fig. 3 that illustrates how QRD-M makes data detection for CP-SC transmissions with binary phase-shift keying (BPSK), $Q = 3$, $M_{\text{QRD-M}} = 2$, $P_T = 1$, and thick-lined branches denoting a set of survivor paths for the next stage processing, where each node has two symbol candidates, $[\boldsymbol{x}]_q = \pm 1$, due to the use of BPSK, the data detection procedure is described as follows:

i) $q = 3$: $\{m_3([\tilde{\boldsymbol{y}}]_3; \mu_3^{(1)}), m_3([\tilde{\boldsymbol{y}}]_3; \mu_3^{(-1)})\}$ respectively compute costs $([\tilde{\boldsymbol{y}}]_3 - [\boldsymbol{R}]_{3,3}([\boldsymbol{x}]_3 = 1))^2$ and $([\tilde{\boldsymbol{y}}]_3 - [\boldsymbol{R}]_{3,3}([\boldsymbol{x}]_3 = -1))^2$ with respect to the received signal $[\tilde{\boldsymbol{y}}]_3$. Since $M_{\text{QRD-M}} = 2$, two branches with $\mu_3^{(1)}$ and $\mu_3^{(-1)}$ are kept for stage $q = 2$.

ii) $q = 2$: In this stage, it is necessary to compute additional costs $([\tilde{\boldsymbol{y}}]_2 - [\boldsymbol{R}]_{2,2}[\boldsymbol{x}]_2 - [\boldsymbol{R}]_{2,3}[\boldsymbol{x}]_3)^2$ with respect to the

received signal $[\tilde{\boldsymbol{y}}]_2$ depending on the values of $[\boldsymbol{x}]_2$ and $[\boldsymbol{x}]_3$. For branches extended from $\mu_3^{(1)}$ that represents $x_3 = 1$, QRD-M computes costs $([\tilde{\boldsymbol{y}}]_2 - [\boldsymbol{R}]_{2,2}[\boldsymbol{x}]_2 - [\boldsymbol{R}]_{2,3}([\boldsymbol{x}]_3 = 1)^2)$ with respect to the received signal $[\tilde{\boldsymbol{y}}]_2$ for $[\boldsymbol{x}]_2 = \pm 1$, that is, $([\tilde{\boldsymbol{y}}]_2 - [\boldsymbol{R}]_{2,2}([\boldsymbol{x}]_2 = \pm 1) - [\boldsymbol{R}]_{2,3}([\boldsymbol{x}]_3 = 1)^2)$ for branches denoted by $\mu_2^{(1,1)}$ and $\mu_2^{(-1,1)}$. Similarly, for branches extended from $\mu_3^{(-1)}$ that represents $[\boldsymbol{x}]_3 = -1$, QRD-M computes costs $([\tilde{\boldsymbol{y}}]_2 - [\boldsymbol{R}]_{2,2}[\boldsymbol{x}]_2 - [\boldsymbol{R}]_{2,3}([\boldsymbol{x}]_3 = -1)^2)$ with respect to the received signal $[\tilde{\boldsymbol{y}}]_2$ for $[\boldsymbol{x}]_2 = \pm 1$, that is, $([\tilde{\boldsymbol{y}}]_2 - [\boldsymbol{R}]_{2,2}([\boldsymbol{x}]_2 = \pm 1) - [\boldsymbol{R}]_{2,3}([\boldsymbol{x}]_3 = -1)^2)$ for branches denoted by $\mu_2^{(1,-1)}$ and $\mu_2^{(-1,-1)}$. Thus, the corresponding accumulated costs up to this stage are given by

$$
\begin{aligned}
&\Delta_{21} \triangleq m_3([\tilde{\boldsymbol{y}}]_3; \mu_3^{(1)}) + m_2([\tilde{\boldsymbol{y}}]_2; \mu_2^{(1,1)}) \text{ for } \mu_2^{(1,1)},\\
&\Delta_{22} \triangleq m_3([\tilde{\boldsymbol{y}}]_3; \mu_3^{(1)}) + m_2([\tilde{\boldsymbol{y}}]_2; \mu_2^{(-1,1)}) \text{ for } \mu_2^{(-1,1)},\\
&\Delta_{23} \triangleq m_3([\tilde{\boldsymbol{y}}]_3; \mu_3^{(-1)}) + m_2([\tilde{\boldsymbol{y}}]_2; \mu_2^{(1,-1)}) \text{ for } \mu_2^{(1,-1)},\\
&\Delta_{24} \triangleq m_3([\tilde{\boldsymbol{y}}]_3; \mu_3^{(-1)}) + m_2([\tilde{\boldsymbol{y}}]_2; \mu_2^{(-1,-1)}) \text{ for } \mu_2^{(-1,-1)}.
\end{aligned} \tag{8}
$$

Among the four accumulated costs, Δ_{22} and Δ_{24} are assumed to be smaller than other two Δ_{21} and Δ_{23}, so that two branches, $\mu_2^{(-1,1)}$ and $\mu_2^{(-1,-1)}$ are kept in addition to Δ_{22} and Δ_{24} for stage $q = 1$.

iii) $q = 1$: In this stage, we extend the branches from $\mu_2^{(-1,1)}$ and $\mu_2^{(-1,-1)}$, that is, $\mu_1^{(1,-1,1)}$, $\mu_1^{(-1,-1,1)}$, $\mu_1^{(1,-1,-1)}$, and $\mu_1^{(-1,-1,-1)}$, and then compute accumulated costs such as

$$
\begin{aligned}
&\Delta_{31} = \Delta_{22} + m_1([\tilde{\boldsymbol{y}}]_1; \mu_1^{(1,-1,1)}) \text{ for } \mu_1^{(1,-1,1)},\\
&\Delta_{32} = \Delta_{22} + m_1([\tilde{\boldsymbol{y}}]_1; \mu_1^{(-1,-1,1)}) \text{ for } \mu_1^{(-1,-1,1)},\\
&\Delta_{33} = \Delta_{24} + m_1([\tilde{\boldsymbol{y}}]_1; \mu_1^{(1,-1,-1)}) \text{ for } \mu_1^{(1,-1,-1)},\\
&\Delta_{34} = \Delta_{24} + m_1([\tilde{\boldsymbol{y}}]_1; \mu_1^{(-1,-1,-1)}) \text{ for } \mu_1^{(-1,-1,-1)}.
\end{aligned} \tag{9}
$$

From Fig. 3, we assume that Δ_{33} has the smallest accumulated costs. Then, QRD-M traces back from stage $q = 1$ to stage $q = Q$ along the path that has the minimum accumulated costs, that is, over the branches $\mu_1^{(1,-1,-1)} \rightarrow \mu_2^{(-1,-1)} \rightarrow \mu_3^{(-1)}$. Thus, the M-algorithm generates the symbol decision of $\boldsymbol{x}$ as $[\boldsymbol{x}]_3 = -1, [\boldsymbol{x}]_2 = -1, [\boldsymbol{x}]_1 = 1$. Note that each of the survivor branches holds its corresponding symbol, so that the QRD-M can make the data detection sequentially by reducing detection error propagation. In addition, the M-algorithm exploits the QRD that generates the upper triangular matrix for the equivalent channel matrix. We can see that $M_{\text{QRD-M}}$ is the key parameter of QRD-M [47] that determines the accuracy of the data detection and the detection complexity. As $M_{\text{QRD}-\text{M}}$ increases, more accurate ML data decision can be obtained.

The original QRD-M was proposed for multiple-input multiple-output (MIMO) OFDM systems [47]. Thus, to use it for CP-SC transmissions, we need to update it as follows:

- In contrast to the OFDM system that applies a data detection for every subcarrier, but individually at a subcarrier, it is necessary to apply QRD-M for a whole symbol block, $\boldsymbol{x} \in \mathbb{C}^{Q\times 1}$, in the TD. With a large value of Q for broadband communications, it is necessary to use a data detection that provides an approximate ML decision with a reduced computational complexity.
- Since the magnitude of the channel frequency response of the MIMO-OFDM system is not equal at every frequency, how to make a best detection order is critical in reducing the detection error propagation since QRD-M can be classified as an extensive version of successive interference cancellation. However, the CP-SC system results in the channel matrix represented by the right circulant matrix, which has the same vector norm for every row channel vector, thus the same data detection performance can be achieved irrespective of the detection order. Thus, the data detection order for QRD-M of the CP-SC system is not so important as that of the MIMO-OFDM system.
- Again from the properties of the right circulant matrix, SNR realized at the QRD-based receiver is given by $\gamma = \rho \sum_{l=1}^{Q} ([\boldsymbol{R}]_{l,l})^2 = \rho \sum_{l=0}^{N_f-1} |h_l|^2$, where $\rho \overset{\triangle}{=} \frac{P_T}{\sigma_z^2}$. Thus, QRD-M can easily achieve this SNR for CP-SC systems with a reasonable value of $M_{\text{QRD-M}}$. However, note that from Table IV, the value of $M_{\text{QRD-M}}$ is not a key parameter in determining the whole computational complexity of the detector when Q is relatively large.

1) QRD-M-based Data Detection for TA-SC and ZP-SC Transmissions: When we apply QRD-M to the TA-SC transmission, $\boldsymbol{H}_{\text{TA}}$ is needed to be decomposed as follows:

$$\boldsymbol{H}_{\text{TA}} = \boldsymbol{Q}_{\text{TA}} \begin{bmatrix} \boldsymbol{R}_{\text{TA},1} & \boldsymbol{R}_{\text{TA},2} \\ \boldsymbol{0}_{N_{\text{UW}}\times Q} & \boldsymbol{R}_{\text{TA},3} \end{bmatrix}$$

where $\boldsymbol{Q}_{\text{TA}} \in \mathbb{C}^{(Q+N_{\text{UW}})\times(Q+N_{\text{UW}})}$ is the unitary matrix, whereas $\boldsymbol{R}_{\text{TA},1} \in \mathbb{C}^{Q\times Q}$ and $\boldsymbol{R}_{\text{TA},3} \in \mathbb{C}^{N_{\text{UW}}\times N_{\text{UW}}}$ are upper triangular matrices. Furthermore, $\boldsymbol{R}_{\text{TA},2} \in \mathbb{C}^{Q\times N_{\text{UW}}}$ is the regular matrix. Since TA-SC appends the UW at the end of $\boldsymbol{x}$, the receiver multiplies the received signal by its processing matrix, $\boldsymbol{Q}_{\text{TA}}^H$. Then, it subtracts the channel effects by the UW. Thus, the updated received signal is given by

$$\tilde{\boldsymbol{y}}_{\text{TA}} = \left[\boldsymbol{Q}_{\text{TA}}^H \boldsymbol{r}_{\text{TA}}\right]_{(1:Q,1)} - \sqrt{P_T}\boldsymbol{R}_{\text{TA},2}\boldsymbol{x}_{\text{TA}} \tag{10}$$

where $\boldsymbol{b} = [\boldsymbol{a}]_{(1:Q,1)}$ denotes a new vector, composed of the first Q elements of $\boldsymbol{a}$. Now using (10) and $\boldsymbol{R}_{\text{TA},1}$, we can directly use QRD-M as that of for CP-SC transmissions. Note that since $\boldsymbol{R}_{\text{TA},3}$ is only related to the UW, it is not used by QRD-M.

Similar to described processing for CP-SC transmissions, it is possible to apply QRD-M to ZP-CP transmissions. When we apply the QRD to $\boldsymbol{H}_{\text{ZP}}$, it is decomposed as follows:

$$\boldsymbol{H}_{\text{ZP}} = \boldsymbol{Q}_{\text{ZP}} \begin{bmatrix} \boldsymbol{R}_{\text{ZP},1} \\ \boldsymbol{0}_{N_{\text{ZP}\times Q}} \end{bmatrix} \tag{11}$$

where $\boldsymbol{Q}_{\rm ZP} \in \mathbb{C}^{(Q+N_{\rm ZP})\times(Q+N_{\rm ZP})}$ is the unitary matrix and $\boldsymbol{R}_{\rm ZP,1} \in \mathbb{C}^{Q\times Q}$ is upper triangular matrix. Note that the zero matrix comes from the over-determined channel matrix. Similar to TA-SC transmissions, we can apply QRD-M with $\boldsymbol{R}_{\rm ZP,1}$ and $\tilde{\boldsymbol{y}}_{\rm ZP} = \left[\boldsymbol{Q}_{\rm ZP}^H \boldsymbol{r}_{\rm ZP}\right]_{(1:Q,1)}$.
For TA-SC transmissions, we can readily verify that the SNR can be equal to that of CP-SC transmissions. Similarly, ZP-SC transmissions result in the same SNR since $([\boldsymbol{R}_{\rm ZP}]_{(1,1)})^2 = \sum_{l=0}^{N_h-1} |h_l|^2$. Thus, QRD-M results in the same performance irrespective of three types of SC transmissions. Some representative papers that apply CP-SC transmissions are listed in Table II for various applications.

2) Achievable Maximum Multipath Diversity Gain by QRD-M-based Data Detection: To understand the achievable multipath diversity, we first need to know the probability density function (PDF) of the realized SNR by the QRD-M. By applying the moment generating function (MGF) and inverse MGF (IMGF), the asymptotic ASER for M-ary phase-shift keying (MPSK), P_e, are derived by $P_e \propto (\rho)^{-N_h}$, which shows an achievable multipath diversity, namely the slope of the ASER is determined by the number of multipath elements. Note that the outage probability can be used to justify the achievable multipath diversity in the considered channel environment.

3) Comparisons with FDE-based Data Detection: The FDE-based receiver transforms the received signal to the frequency domain (FD) by applying the DFT. After applying the minimum mean-square error (MMSE)-based equalizer in the FD, that is called FDE, an inverse DFT (IDFT) is applied to transform its equalized signal back to the TD. Then, a detector is applied to recover the original signal. With the use of CP/UW/zero padding and FDE, SC is robust to delay spread. Thus, SC with FDE, called SC-FDE, has been recognized as a practical technique in mitigating the time-dispersive effects in frequency selective fading channels. It has been reported that it can provide the similar performance as that of OFDM. However, a primary challenging problem with SC-FDE is that they do not provide a reliable performance in frequency selective fading channels due to a limited achievable multipath diversity for the systems with uncoded SC transmissions [48], [49].

The computational complexities of the MLD, QRD-M, and MMSE-based FDE are provided in Table IV. In this table, we define $\boldsymbol{W} \triangleq (\boldsymbol{H}_{\rm CPSC}\boldsymbol{H}_{\rm CPSC}^H + \sigma_z^2 \boldsymbol{I}_Q)^{-1}\boldsymbol{H}_{\rm CPSC}^H$, and recall that C denotes the size of the signal constellation. In particular, this table shows that QRD-M has almost half complexity than MMSE-based SC-FDE. However, QRD-M can significantly reduce the computational complexity of MLD that exponentially increases as Q increases. Note that latency is the time required for the transmission of a packet over a channel. However, with very stringent latency requirements and complexity constrained receivers, the time required for the decoding of the packet cannot be ignored and must be included in the total latency analysis [50]. Thus, QRD-M can reduce the decoding related latency by half compared with SC-FDE.

TABLE IV

COMPUTATIONAL COMPLEXITY OF THE DETECTORS IN TERMS OF THE NUMBER OF REAL MULTIPLICATIONS.

detector	operations	number of real multiplications	total number of real multiplications
MLD	computation: $\boldsymbol{H}_{\text{CPSC}}\boldsymbol{x}$	$4Q^2.C$	$\approx 2Q.C^Q$
	computation: $\|\boldsymbol{y}-\boldsymbol{H}_{\text{CPSC}}\boldsymbol{x}\|^2$	$2Q.C^Q$	
QRD-M	computation of QRD: $\boldsymbol{H}_{\text{CPSC}}=\boldsymbol{QR}$	$4Q^3$	$\approx 4Q^3$
	computation:$\tilde{\boldsymbol{y}}=\boldsymbol{Q}^H\boldsymbol{y}$	$4Q^2$	
	computation: $\sqrt{P_T}\boldsymbol{Rx}$	$4Q.((Q+1)/2).C$	
	computation:$\|\tilde{\boldsymbol{y}}-\sqrt{P_T}\boldsymbol{Rx}\|^2$	$2C.Q.M_{\text{QRD-M}}$	
MMSE-based SC-FDE	computation: $\boldsymbol{W}$ and $\hat{\boldsymbol{r}}\triangleq\boldsymbol{W}\tilde{\boldsymbol{r}}$	$4(2Q^3+Q.(Q+1)^2)+4Q^2$	$\approx 8Q^3$
	computation: $\tilde{\boldsymbol{r}}\triangleq\boldsymbol{Fr}$ and $\boldsymbol{F}^H\hat{\boldsymbol{r}}$	$2.4Q^2$	

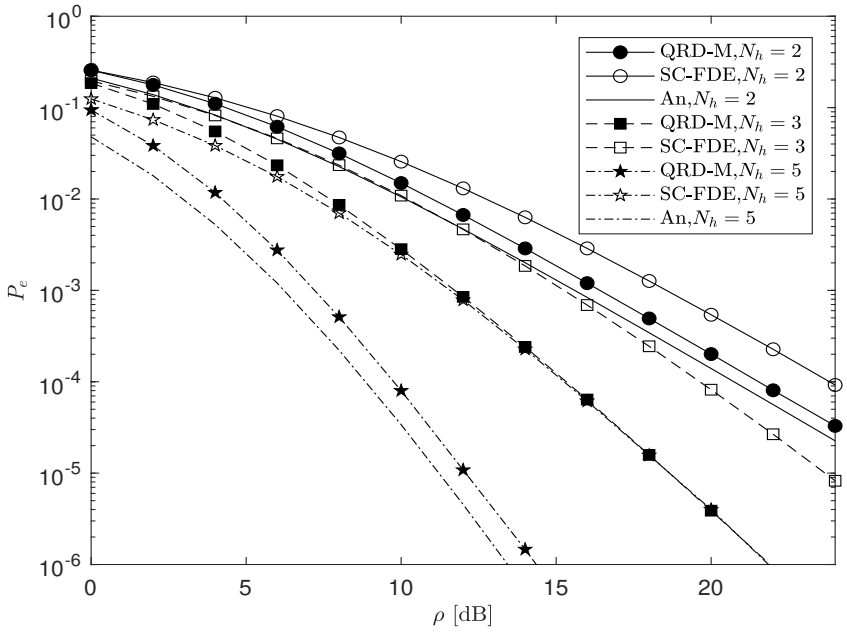

Fig. 4. ASER of CP-SC transmissions. In this simulation, N_h denotes the number of multipath of $\boldsymbol{h}$.

4) Verification of Achievable Multipath Diversity by QRD-M-based Data Detection: We compare the ASER of CP-SC, ZP-SC, and TA-SC with $Q=128$, $N_{\text{CP}}=N_{\text{ZP}}=N_{\text{UW}}=16$, $M_{\text{QRD-M}}=32$, and QPSK modulation. For various sizes of the channel vector, $\boldsymbol{h}$, QRD-M and SC-FDE with the MMSE-based equalizer are employed at the receiver. In the following Figs. 4 and 5 also include the analytically obtained ASER denoted by An. This curve

exactly shows the achievable full diversity.

In particular, in Fig. 4, we mainly consider CP-SC transmissions and compare the ASER of the receivers that respectively employ QRD-M and SC-FDE. This figure shows that QRD-M allows the receiver to achieve a better ASER performance than the receiver with SC-FDE as N_h increases. In addition, it is shown that QRD-M allows the receiver to achieve multipath diversity, N_h, in the high SNR region. However, the receiver with SC-FDE can achieve only a partial multipath diversity [20]. Thus, we suggest the following corrections.

- The authors of [51] asserted that the block size is a factor that determines the achievable maximum multipath diversity. However, if we can achieve ISI-free reception at the receiver by imposing the condition $N_h \geq |\boldsymbol{h}|$, the block size has no influence on the achievable maximum multipath diversity.

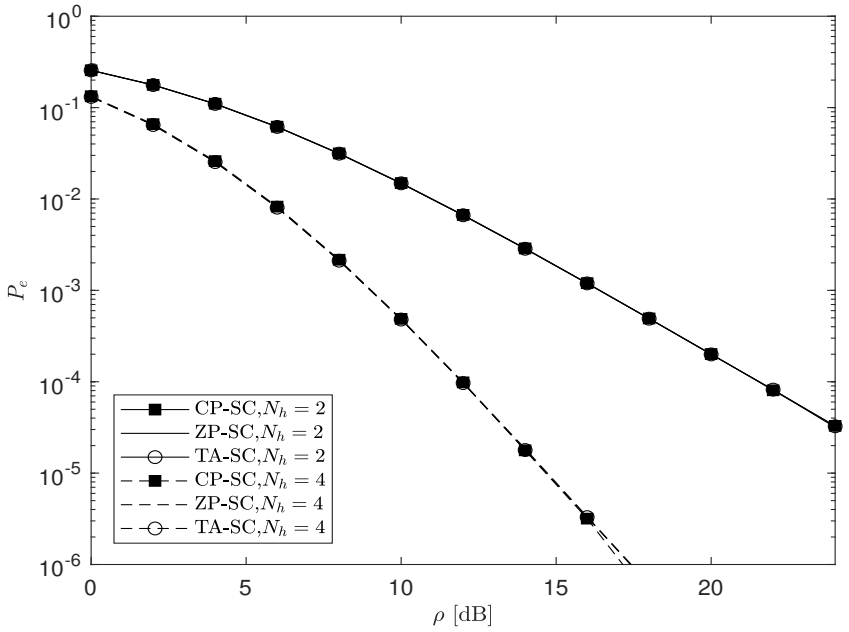

Fig. 5. ASER of CP-SC, TA-SC, and ZP-SC transmissions. QRD-M is employed at the receivers.

Furthermore, Fig. 5 shows that the receiver that employs QRD-M results in the same ASER irrespective of the type of SC transmissions. Thus, it is hard to distinguish the curves in Fig. 5. From Figs. 4 and 5, we can summarize the following new observations.

- The authors of [52] asserted that TA-SC transmissions result in the better performance than CP-SC transmissions. However, if we follow pre-processing for QRD-M as described in ahead, CP-SC transmissions can result in the same performance as those of TA-SC transmissions.

- Although the authors of [42], [52] verified the performance of TA-SC transmissions with the QRD-M-based data detection, they do not provide achievable diversity. Thus, Fig. 5 verifies that the full multipath diversity can be achieved by the QRD-M-based data detection.

Since performance differences are not expected between CP-SC, TA-SC, and ZP-SC transmissions, we will mainly focus on CP-SC transmissions in the sequel.

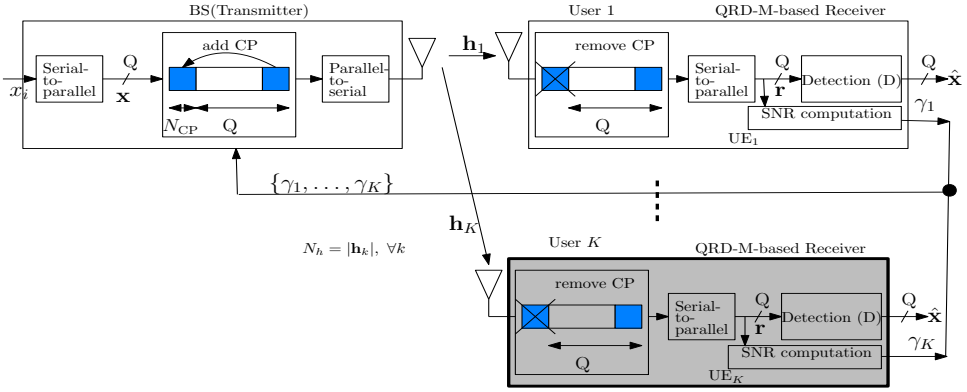

Fig. 6. CP-SC with opportunistic user scheduling. We assume that there are K users in the system. A highlighted user is selected for data transmissions.

5) Achievable Multiuser Diversity by QRD-M-based Data Detection: We can verify achievable multiuser diversity by using the opportunistic user scheduling illustrated in Fig. 6. For the wireless communication system comprised by the one base station (BS) and K distinct users, the transmission is divided into two phases, namely pilot transmission phase and data transmission phase.

- First pilot transmission phase: Each user measures its realized SNR by its receiver operation, $\{\gamma_1, \ldots, \gamma_K\}$, each of which is given by $\gamma_j \triangleq \rho \|\boldsymbol{h}_j\|^2$, based on the pilot symbols, then feeds back it to the BS.
- Second data transmission phase: After receiving a set of SNRs from all users, $\{\gamma_1, \ldots, \gamma_K\}$, the BS selects a user who will realize the greatest SNR by data transmissions, for example, K in Fig. 6, that is $K = \arg\max_j(\gamma_j)$.
- To verify multiuser diversity, we provide Fig. 7. Combining CP-SC transmissions with the proposed opportunistic user scheduling in the considered channel environment, we can verify that the full multiuser diversity can be effectively exploited by lowering the outage probability. For example, $(N_h = 2, K = 3)$ vs $(N_h = 2, K = 6)$. Thus, high-reliable communications can be achieved. Furthermore, multipath diversity can be observed as well by comparing the scenario $(N_h = 3, K = 2)$ with $(N_h = 6, K = 2)$. However, the same

slope is observed for $(N_h = 2, K = 3)$ vs $(N_h = 3, K = 2)$ since the maximum diversity is expressed by the multiplication of multipath diversity and multiuser diversity.

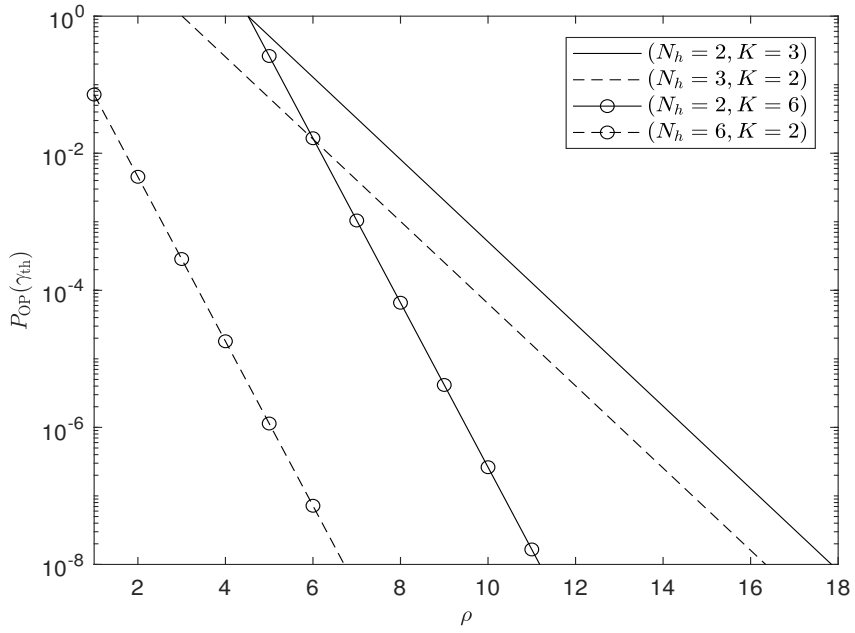

Fig. 7. Outage probability in terms of N_h and the number of users K. We use a fixed 1 dB threshold for γ_{th}.

6) Transmit Diversity by dCDD and QRD-M-based Data Detection: One of the well exploited transmit diversity techniques is cyclic delay diversity (CDD) that transmits the same block symbol from the multiple antennas with employing a different cyclic delay at each antenna. In CDD-based CP-SC systems, equipped with n_T transmit antennas, $n_T - 1$ copies of a block symbol, $\boldsymbol{x}$, are generated by shifting $\boldsymbol{x}$ up to a given cyclic delay. The primary objective of CDD is to convert the multiple-input single-output (MISO) channel into the single-input single-output (SISO) channel, i.e., converting spatial diversity to frequency diversity. However, since CDD results in performance variation over the subcarriers, FEC coding is usually required to exploit frequency diversity in OFDM systems. In contrast, we can verify that CP-SC systems do not require to employ FEC coding to achieve frequency diversity. Using the benefits of CDD, we can exemplify one dCDD-based system in Fig. 8, composed by a set of distributed and cooperating transmitters or remote radio heads (RRHs). Note that in a different architecture, the RRH can work as the gNodeB (gNB)-CU while the distributed units (DUs) can work as RRHs, that is, the DUs are connected to the gNB-CU that provides support for the higher layers of the protocol. Under an assumption of tight time and frequency synchronization among RRHs and taking into account the propagation delays, N_{CP} can be determined

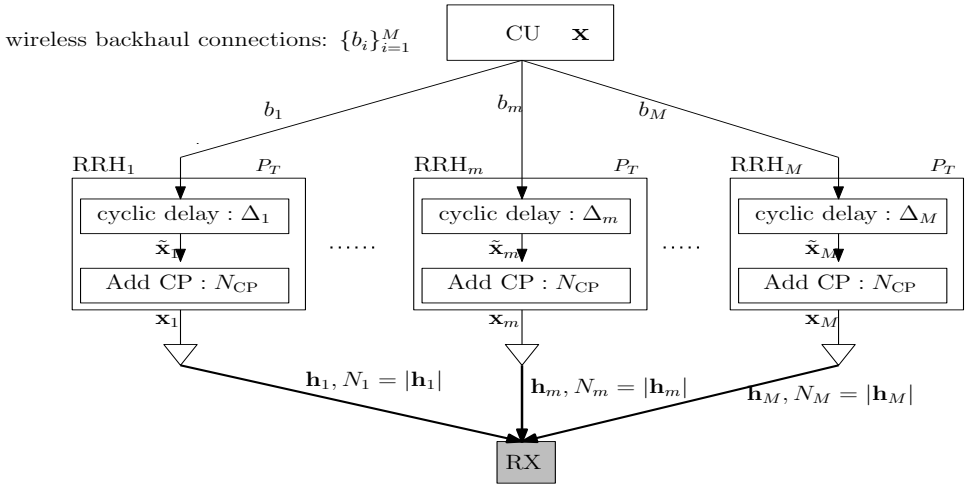

Fig. 8. Illustration of the under-populated dCDD-based CP-SC system, composed by one CU, M RRHs, and one RX.

to remove ISI caused by all the RRHs and exploit the full diversity. Thus, the primary advantage of dCDD is to exploit the full diversity without requiring full CSI at the transmitting side and FEC coding.

Extending the systems, illustrated in Fig. 2, CP-SC transmissions for dCDD need to be redefined as follows:

- For the input transmission block symbol $\boldsymbol{x}$, RRH$_m$ applies its cyclic delay, Δ_m to $\boldsymbol{x}_m$, that is, $\boldsymbol{x}_m = [x_{Q-\Delta_m+1}, \ldots, x_Q, x_1, x_2, \ldots, x_{Q-\Delta_m}]^T$. This is expressed by $\boldsymbol{x}_m = \boldsymbol{P}_{\Delta_m}\boldsymbol{x}$ with the permutation shifting matrix $\boldsymbol{P}_{\Delta_m}$, which is obtained from $\boldsymbol{I}_Q$ by circularly shifting down by Δ_m. For instance, for $Q = 4$, $\boldsymbol{P}_{\Delta_m=2}$ is defined by $\boldsymbol{P}_{\Delta_m=2} = \begin{bmatrix} 0 & 0 & 1 & 0 \\ 0 & 0 & 0 & 1 \\ 1 & 0 & 0 & 0 \\ 0 & 1 & 0 & 0 \end{bmatrix}$. Then, RRH$_m$ appends the CP, determined by $\boldsymbol{x}_m$, to the transformed transmission block symbol $\boldsymbol{x}_m$ before the transmission via its antenna.
- Since there are M simultaneous CP-SC transmissions from M RRHs, the received signal at the RX is given by $\boldsymbol{y} = \sqrt{P_T}\sum_{m=1}^M \boldsymbol{H}_m\boldsymbol{P}_{\Delta_m}\boldsymbol{x} + \boldsymbol{z}$, where $\{\boldsymbol{H}_m\}_{m=1}^M$ is the set of right circulant channel matrices respectively determined by $\boldsymbol{h}_m$. When we do not apply additional operation at each RRH, ISI will be resulted in the RX.

To exploit the full diversity, it is necessary to have ISI-free reception at the RX, so that two conditions should be met as follows:

- $\Delta_m = (m-1)N_{\mathrm{CP}}, m = 1, \ldots, M$, where $N_{\mathrm{CP}} = \max(N_1, \ldots, N_M)$, with N_m denoting the number of multipath components of the channel $\boldsymbol{h}_m$ from the mth RRH to RX.
- $K = \lfloor Q/N_{\mathrm{CP}} \rfloor$.

The first condition is required to avoid ISI cased by multipath channels, whereas the second condition is required

to avoid ISI caused by simultaneous multiple CP-SC transmissions considering the size of the symbol block $\boldsymbol{x}$. Thus, these two conditions make CP-SC systems overcome challenging problems in achieving transmit diversity or macro diversity by the distributed devices/nodes in the considered channel environment.

To illustrate ISI-free reception by dCDD, we provide one example as follows: Let us assume that $Q = 6, K = 2, N_1 = 2$, and $N_2 = 3$. Then, by the use of dCDD, an equivalent channel matrix $\boldsymbol{H}_{\mathrm{CPSC}}$ is given by

$$\boldsymbol{H}_{\text{dCDD}} = \begin{bmatrix} h_{1,1} & h_{2,3} & h_{2,2} & h_{2,1} & 0 & h_{1,2} \\ h_{1,2} & h_{1,1} & h_{2,3} & h_{2,2} & h_{2,1} & 0 \\ 0 & h_{1,2} & h_{1,1} & h_{2,3} & h_{2,2} & h_{2,1} \\ h_{2,1} & 0 & h_{1,2} & h_{1,1} & h_{2,3} & h_{2,2} \\ h_{2,2} & h_{2,1} & 0 & h_{1,2} & h_{1,1} & h_{2,3} \\ h_{2,3} & h_{2,2} & h_{2,1} & 0 & h_{1,2} & h_{1,1} \end{bmatrix} \tag{12}$$

where $h_{j,i}$ denotes the ith element of $\boldsymbol{h}_j$.

- From the representation of (12), assigned cyclic delays are $\Delta_0 = 0$ and $\Delta_1 = 3$, that is, $\boldsymbol{P}_{\Delta_0} = \boldsymbol{I}_Q$. However, $\boldsymbol{P}_{\Delta_1}$ is obtained from $\boldsymbol{I}_Q$ by shifting down three for all rows of $\boldsymbol{I}_Q$. In particular, from (12), we can see that non-overlapped channel elements are observed in each of the components of $\boldsymbol{H}_{\text{dCDD}}$.
- When the two mentioned conditions are met, the received signal becomes $\boldsymbol{y} = \sqrt{P_T}\boldsymbol{H}_{\text{dCDD}}\boldsymbol{x} + \boldsymbol{z}$, which has a similar form as those of non-dCDD supported CP-SC transmissions. Thus, the channel utilization is much improved by dCDD.
- dCDD can effectively handle multiple K simultaneous CP-SC transmissions without causing ISI at the RX. By employing QRD-M at the RX, multiuser diversity can be achieved even in the considered channel environment.

However, since the second condition is constrained by the symbol size, Q, we can categorize its operation into two modes depending on K and M: over-populated ($K < M$) and under-populated ($K \geq M$).

- Over-populated system, i.e., $K < M$: Since only K RRHs support dCDD to exploit the full achievable diversity, the CU needs to know information fed back from the RX. Based on a very reliable channel estimate, the RX can determine the order of channel magnitude as follows: $\|\boldsymbol{h}_{(1)}\|^2 > \ldots > \|\boldsymbol{h}_{(M)}\|^2$. Furthermore, the RX can readily determine the number of multipath components, $(N_1, \ldots, N_M)$, for the channels connected with M RRHs. Then, the RX feeds back a list $\mathbb{I} = ((1), \ldots, (M))$ that specifies the order of channel magnitude and $N_{\mathrm{CP}} = \max(N_1, \ldots, N_M)$. Upon receiving $\mathbb{I}$ and N_{CP}, the CU assigns cyclic delays only to K RRHs, which are indexed by the first K elements of $\mathbb{I}$. To avoid ISI from multiple CP-SC transmissions, un-selected RRHs are refrained from transmissions. Thus, a kind of opportunistic user scheduling described in Section II-B-(5) is employed.
- Under-populated system, i.e., $K \geq M$: In contrast to the over-populated system, all the M RRHs take part in dCDD operation. For the block symbol, $\boldsymbol{x}$, the CU assigns the cyclic delay, Δ_m, to RRH$_m$. After assigning the cyclic delay, RRH$_m$ appends the CP to obtain $\boldsymbol{x}_m$ before its transmissions.

- Under/Over-populated system: By virtue of the property of the equivalent channel matrix $\boldsymbol{H}_{\mathrm{CPSC}}$, which is right circulant, the performance of CP-SC systems that employs the dCDD depends on the realized SNR, expressed by $\gamma \overset{\triangle}{=} \rho \sum_{m=1}^{M} \sum_{i=0}^{N_{\mathrm{CP}}-1} |h_{m,i}|^2$, with $\rho \overset{\triangle}{=} \frac{P_T}{\sigma_z^2}$ and $h_{m,i}$ denoting the ith element of $\boldsymbol{h}_m$, the channel vector from the mth RRH to RX, respectively. When $N_m \leq N_{\mathrm{CP}}$ zero padding is applied to $\boldsymbol{h}_m$. Thus, multipath diversity, N_{CP}, and multiuser diversity, M, can be exploited as transmit diversity by the dCDD. As was explained in Sections II-B-(4) and II-B-(5), the use of QRD-M is necessary to achieve multipath and multiuser diversity simultaneously, eventually transmit diversity.

  Similar to the under-populated system, the SNR realized at the RX of the over-populated system is given by $\gamma = \rho \sum_{k=1}^{K} \sum_{l=0}^{N_{\mathrm{CP}}-1} |h_{(k),l}|^2$. Since the realized SNR is composed by K respective greater SNRs by referring to a list $\mathbb{I}$, the full diversity can be exploited in time dispersive fading channels. Since the CU selects K RRHs for dCDD according to the list $\mathbb{I}$, the CU is able to choose K RRHs that result in the greatest sum of the realized SNRs at the RX. In other words, the list $\mathbb{I}$ includes the index of the $\mathrm{RRH}_{(1)}$ that results in the greatest realized SNR at the RX, so that the maximum achievable multiuser diversity is similar to that of the system that employs opportunistic user scheduling. Thus, the maximum achievable diversity is MN_m rather than KN_m. This can be measured from the slope of the outage probability curve.

  Referring to Fig. 9, we can see that various over-populated distributed CP-SC systems with $M = 3$ RRHs can effectively exploit the full diversity. That is, although three RRHs exist in the system, only $K \leq M$ RRHs are used for CP-SC transmissions by dCDD. We can see the following observations: i) Although the scenario $(K = 2, N = 1)$ supports more RRHs for dCDD, its slope is almost the same as that of the scenario $(K = 1, N = 1)$ because the maximum diversity is the same irrespective of K [1]; ii) The scenario $(K = 2, N = 2)$ results in twice the slope of the scenario $(K = 2, N = 1)$ due to a greater multipath diversity, which is determined by N; iii) We can see that the maximum multiuser diversity is determined by the total number of RRHs in the system in over-determined system; and iv) The maximum diversity can be achievable by dCDD even in the over-populated system depending on the total number of RRHs rather than the number of dCDD RRHs, which is a more popular setup in distributed wireless systems.

In summary, QRD-M-based data detection can achieve different types of diversity, such as multipath diversity, multiuser diversity, and transmit diversity, in the considered environment over the frequency selective fading channel. In the next Section, we will exemplify some successful CP-SC-based wireless communication systems that exploit these different types of diversity by enabling cooperating among distributed devices/nodes in the challenging and realistic channel environment.

[1]However, a lower outage probability is obtained as K increases due to coding gain.

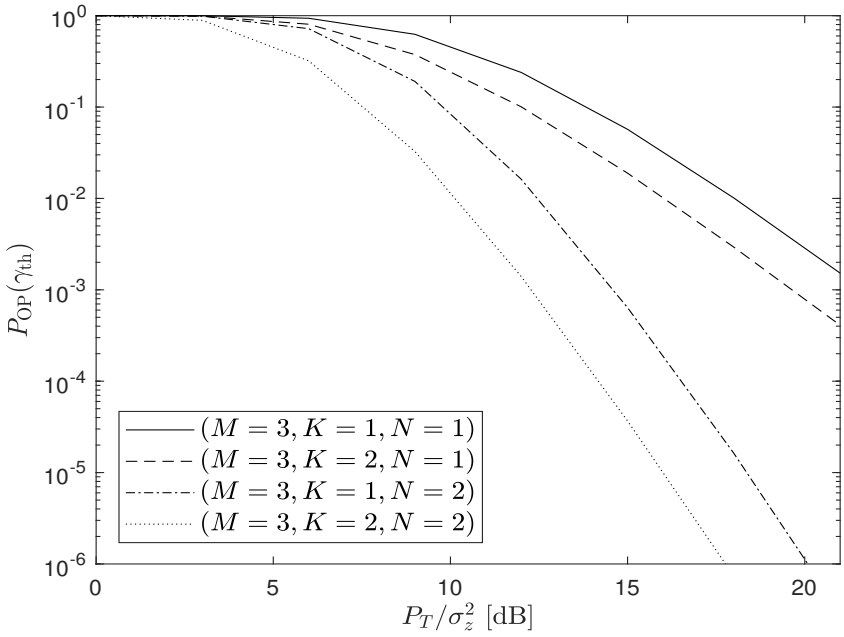

Fig. 9. Outage probability in terms of $(M, K, N = \{N_m\}_{m=1}^{M})$.

III. Successful Applications of CP-SC in Cooperative Communications

A. Relaying Systems

Some of the disadvantages of communications targeting at increasing the coverage area are as follows:

- The higher power consumption is required for transmissions power.
- Large interference can be introduced from the neighboring cells.
- Reliable transmissions can not be guaranteed at the cell edge due to large path loss and shadowing fading.

To cope with these problems, cooperative relaying communications [53]–[55], where multiple relaying nodes assist the source node to transmit symbols to the destination nodes, have been proposed. Since the existence of the relaying nodes means an increasing operating area of communications, it is necessary to improve the performance of the relaying system to maintain very reliable communications over this operating area. Thus, we will illustrate how CP-SC transmissions can be applied to increase performance of relaying communications.

The concept of multihop relaying networks has been foreseen as a promising communication mechanism to expand network coverage [56], [57], and achieve better transmission performance for wireless sensor networks and mobile ad-hoc networks [58]–[60]. However, multihop relaying protocols need to be integrated in cooperative communications to cover wide area operation and support multi-Gbps data rates by collaborating among many heterogeneous stationary, ad-hoc, and mobile devices [61].

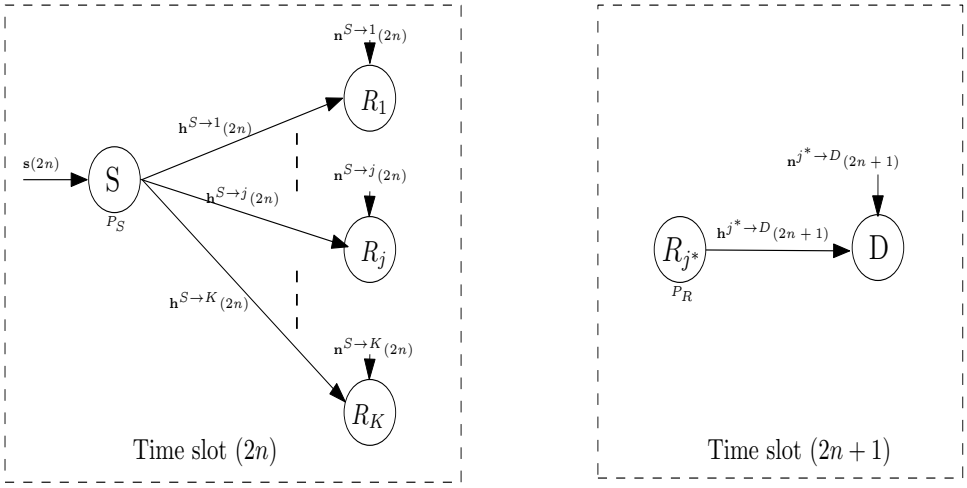

Fig. 10. AF-based CP-SC relaying system with best relay selection (BRS).

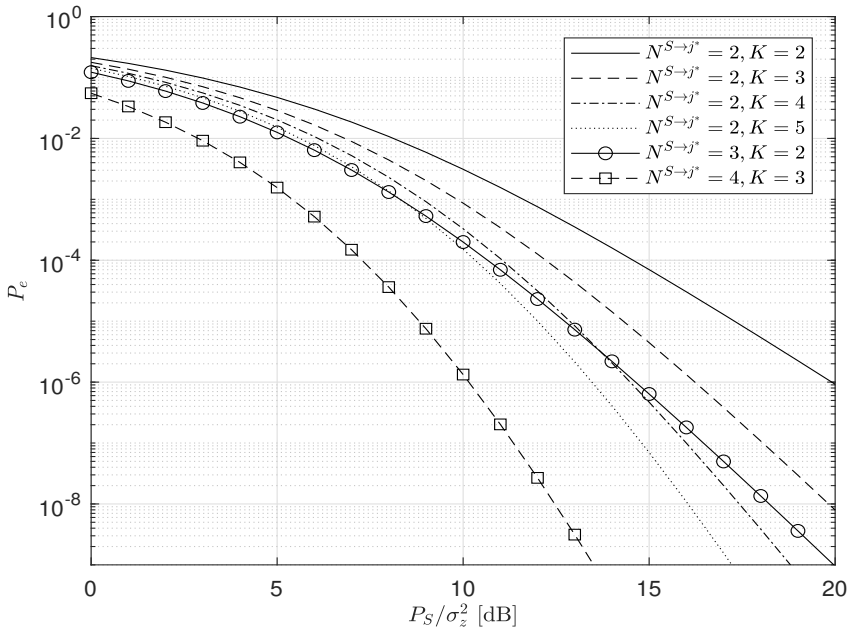

Fig. 11. ASER for various values of $N^{S\to j^*}$ and K.

We exemplify one cooperative relaying system provided in Fig. 10, where K relaying nodes, $\{R_1, \ldots, R_K\}$, coexist with a single source (S) and destination node (D). Each amplify-and-forward (AF) relaying node simply amplifies and re-transmits the signal to D without decoding. We can summarize its relaying operation composed by the pilot symbol block operation and data symbol block operation, and performance as follows:

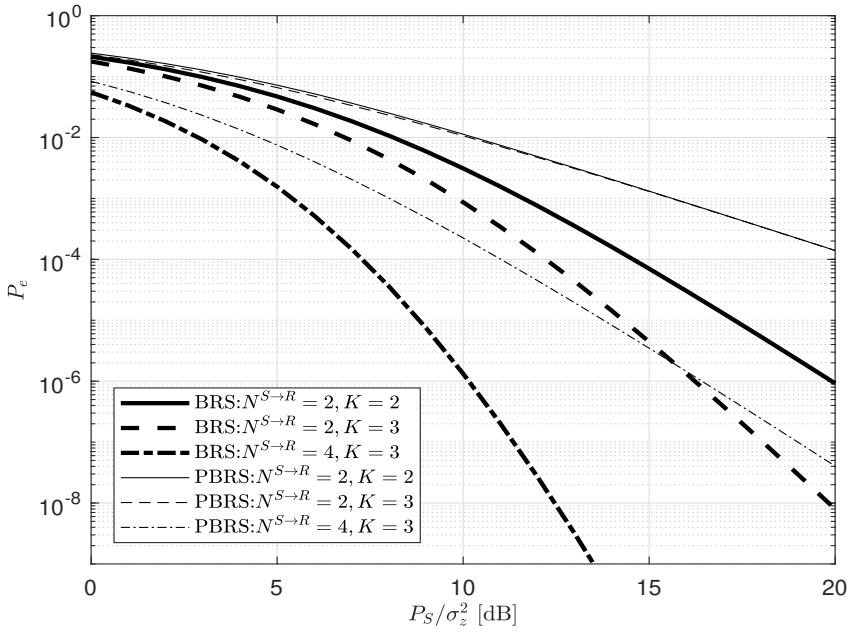

Fig. 12. ASER comparison of the CP-SC-based relaying systems with BRS and PBRS for various values of $N^{S\to R}, R=\forall R_j$ and K.

- Operation for the pilot symbol block: The destination node D measures the SNR realized by CP-SC transmissions over the channels from S to R_j and from R_j to D. Note that $N^{S\to j}$ and $N^{j\to D}$ respectively denote the numbers of multipath components of $\boldsymbol{h}^{S\to j}$ and $\boldsymbol{h}^{j\to D}$. Let $\gamma_{S\to j}=\frac{P_S\|\boldsymbol{h}^{S\to j}\|^2}{\sigma_z^2}$ be the realized SNR by CP-SC transmissions over the channel from S to R_j. Similarly, let $\gamma_{j\to D}=\frac{P_R\|\boldsymbol{h}^{j\to D}\|^2}{\sigma_z^2}$ be the realized SNR by CP-SC transmissions over the channel from R_j to D. Then, due to the use of AF relaying protocol, the end-to-end realized SNR over the channel from S to R_j and from R_j to D is proportional to $\gamma_j \propto \frac{\gamma_{S\to j}\gamma_{j\to D}}{\gamma_{S\to j}+\gamma_{j\to D}+1}$. Due to a handshaking between R_js and D, $\{\gamma_{S\to j}\}_{j=1}^K$ are assumed to be known at D by the use of the pilot symbol block. Among K individually measured end-to-end SNRs, $\{\gamma_j\}_{j=1}^K$, D selects the relay, R_{j^*}, that realizes the greatest SNR, that is, $j^*=\arg\max_j(\gamma_j)$, and feeds back its index, j^*, to S via backhauls connected from D to R_{j^*} and from R_{j^*} to S. Note that the equivalent channels become again right circulant matrices respectively determined by $\boldsymbol{h}^{S\to j}$ and $\boldsymbol{h}^{j\to D}$. Time sensitive networking (TSN) can be used as a link layer protocol for reliable and low latency communication for wired backhaul connections [37]. Thus, the development of the wireless TSN was initiated to support wireless backhaul connections.
- Operation for the data symbol block: CP-SC data transmissions are accomplished via only the selected relay R_{j^*}. Thus, CP-SC transmissions are made via from S to R_{j^*} and then from R_{j^*} to D in two time slots.
- We can show that this cooperative relaying system can exploit the full diversity. For various values of $N^{S\to j^*}$

and K, Fig. 11 shows that this considered cooperative relaying systems with the AF relaying protocol can effectively exploit the full diversity by reducing the ASER, which eventually increases reliability of CP-SC transmissions. For link-level simulations, we assume that $N^{S\to j^*} = N^{j^*\to D}$ and $P_S = P_R = 1$. When we fix $N^{S\to j^*} = 2$, then a better ASER is obtained as K increases due to a greater multiuser diversity. However, when we fix $K = 2$, a better ASER is obtained as $N^{S\to j^*}$ increases due to a greater multipath diversity. Jointly taking into account of these observations, $(N^{S\to j^*} = 3, K = 3)$ results in the best ASER performance, whereas $(N^{S\to j^*} = 2, K = 2)$ results in the worst ASER performance due to its least achievable full diversity. Thus, CP-SC transmissions benefit from the multipath diversity compared to non-CP-SC transmissions in the considered frequency selective fading channel environment. Note that since the source node needs to know only the relay index, the destination node is not necessary to feed back full CSI.

- Using the concept of partial selection mechanism, we can use only CSI for the links between the source and all the relaying nodes to select the best relay for data transmissions [62]. For the system illustrated in Fig. 10, R_{j^*} is selected by means of $j^* = \arg\max_j(\gamma_{S\to j})$. Note that this relay selection is also determined by the use of the pilot symbol block. This is called the partial best relay selection (PBRS) scheme. To reduce the implementation cost and required complexity, this can be employed in ad-hoc and sensor cooperative networks [63]. Since the link from the selected relay to destination is not considered, a loss in the achievable full diversity occurs, namely from the full diversity to a partial diversity, which is verified by link-level simulations illustrated in Fig. 12, where we assume that $N^{S\to R} = N^{R\to j}$ and $P_S = P_R = 1$. In particular, a similar observation can be made in terms of $(N^{S\to R}, K)$ as that of Fig. 11. When we compare the ASER performance for relay selection either by BRS or PBRS, a performance loss is observed with PBRS due to a loss in the full diversity. Thus, to reduce the implementation cost, PBRS sacrifices high-reliable transmissions capability.
- In summary, BRS can be recognized as an alternative opportunistic user selection explained in Section II-B-(5). In contrast, PBRS is a practical version of opportunistic user selection.

We can exemplify another cooperative relaying system that achieves the full diversity [26], where one relaying node, R, and K terminals, $\{T_1, \ldots, T_K\}$, are assumed to be coexist in the relaying network as illustrated in Fig. 13, where $N^{S\to R}$ and $N^{R\to j}$ respectively denote the number of multipath components of $\boldsymbol{h}^{S\to R}$ and $\boldsymbol{h}^{R\to j}$. We can also summarize its relaying operation composed by the pilot symbol block operation and data symbol block operation, and performance as follows:

- Operation for the pilot symbol block: A terminal T_j measures its realized SNR, $\gamma_j = \frac{P_R\|\boldsymbol{h}^{R\to j}\|^2}{\sigma_z^2}$ over the channel $\boldsymbol{h}^{R\to j}$, and feeds back it to R via a backhaul connected to R.
- Operation for the data symbol block: Based on available K received SNRs, $\{\gamma_j\}_{j=1}^K$, R selects only one terminal, T_{j*}, that realizes the greatest SNR for data transmissions, that is, $j^* = \arg\max_j(\gamma_j)$.
- When QRD-M is employed at relaying and every terminal nodes, Fig. 14 verifies that this relaying system can

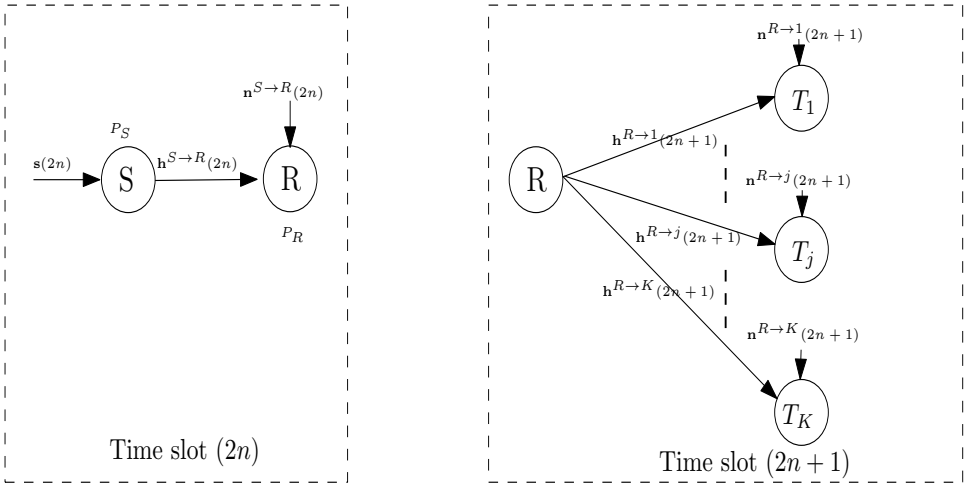

Fig. 13. AF-based CP-SC relaying system with opportunistic best terminal selection (BTS).

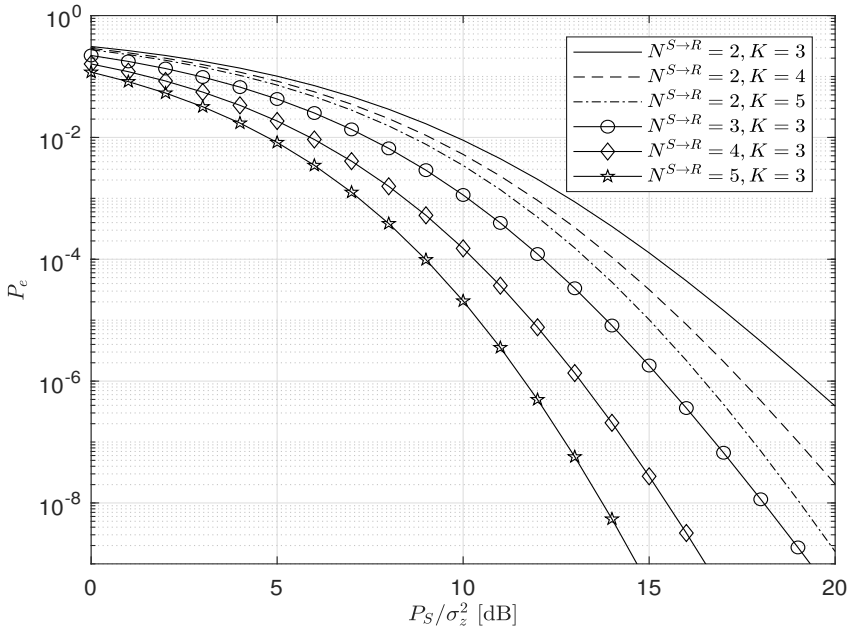

Fig. 14. ASER for various values of $N^{S\to R}$ and K.

exploit the full diversity in the considered channel environment to decrease the ASER. For example, $(N^{S\to R}=2, K=3)$ vs $(N^{S\to R}=4, K=3)$ for the verification of multipath diversity and $(N^{S\to R}=2, K=3)$ vs $(N^{S\to R}=2, K=4)$ for the verification of multiuser diversity. For link-level simulations, we assume that $N^{S\to R}=N^{R\to j}$ and $P_S=P_R=1$.

- In summary, the illustrated BTS is a further extension of the opportunistic scheduling in the cooperative relaying network. As in the previous relaying system, cooperative relaying systems benefit from CP-SC transmissions to achieve high-reliable transmissions in a wide coverage area rich with frequency selective fading channels.

B. Spectrum Sharing Systems

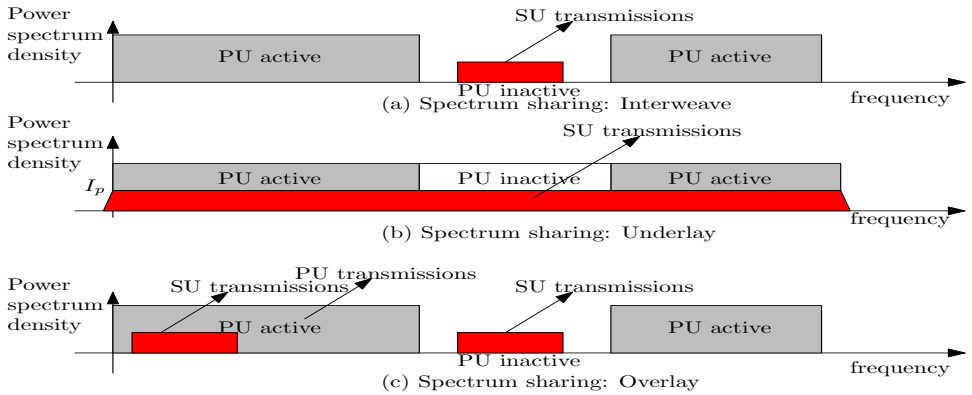

Fig. 15. Three different types of spectrum sharing.

A conventional spectrum management focuses on how to partition the radio spectrum into fixed frequency bands allocated to a specific wireless technology to ensure that frequency bands are available when they are needed. Although the conventional spectrum management is easy to be implemented, it is inefficient in managing the scarce natural radio spectrum. Many measurement campaigns conducted all over the world have demonstrated that a large amount of licensed radio spectrum is inefficiently utilized due to the existence spatial and temporal holes, see e.g., [64]. Spatial holes are resulted from an inefficient geographical use of radio spectrum, whereas temporal holes are caused from an inefficient periodic use of radio spectrum. To counter these inefficient use of radio spectrum, the cognitive radio (CR) network was proposed by the author of [65]. How the SU is allowed to access spectrum, three different types of spectrum sharing [66], namely, overlay [67], underlay [68]–[70], and interweave [71] have been proposed. Spectrum sharing is an effective in implementing dynamic spectrum management [72]. TV White Space (TVWS) is one typical real world test example [73]. It is managed by a geolocation database, which controls TVWS device frequencies and transmission power so that the devices do not interfere with other wireless communication systems including terrestrial TV service. In the interweave spectrum sharing, illustrated in Fig. 15-(a), the SU is not allowed to cause any interference to the PU network, so that it needs to sense spectrum occupancy periodically [71]. Thus, when the PU is not active for a specific spectrum, the SU can access for its transmissions. In the overlay spectrum sharing [67], illustrated in Fig. 15-(c), the SU is allowed to use spectrum, which is assigned to a licensed PU when the spectrum is free to access. Thus, the secondary network is required to correctly detect whether target

spectrum is unoccupied [74] and then immediately release the channel when the PU wants to use target spectrum [75].

In underlay spectrum sharing, illustrated in Fig. 15-(b), the SU can co-occupy target spectrum as long as its interference to the PU is under a threshold, I_p, i.e., it does not cause significant harmful interference to the PU [27], [68], [69].

Since the spectrum sharing network must limit its transmit power to minimize its interference influencing the capability of PU in accessing spectrum, constraint χ_1, the performance of the secondary network will be degraded. In addition to the constraint χ_1, an advanced spectrum sharing system considers maximum transmit power P_T at the SU-source (SU-S) and SU-relays, $\{\text{SU-R}_j\}_{k=1}^{K}$, constraint χ_2, which is more effective in protecting the PU receiver.

Ever since CP-SC transmissions were proposed by [27] and [69], CP-SC transmissions have been applied to efficiently use limited radio spectrum. In particular, how to develop spectrum agile systems and management that increase spectrum access capability is also an important question in 5G systems. To answer to this question, we will introduce how benefits from CP-SC transmissions can be used for spectrum sharing in the sequel.

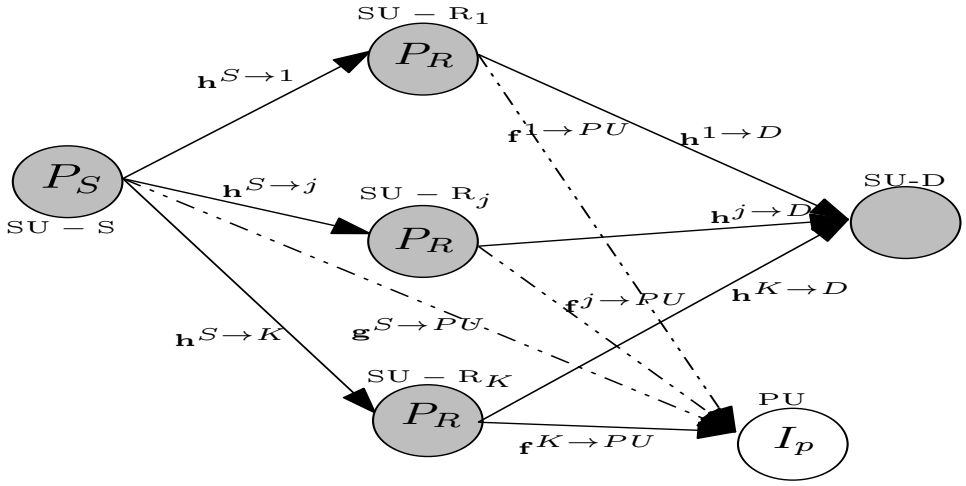

Fig. 16. Illustration of the CP-SC spectrum sharing system with the decode-and-forward (DF) relaying protocol. K SU-relays, $\{\text{SU-R}_j\}_{k=1}^{K}$, and PU are assumed in the system. The SU network is composed by the SU-S, SU-relays, and SU-destination (SU-D).

- For the spectrum sharing system illustrated in Fig. 16, we can apply two types of relay selection, namely BRS and PBRS, described in Section III-A-(1), for the CP-SC spectrum sharing system with the DF relaying protocol [69]. In contrast to the AF relaying protocol, each DF relaying node decodes, re-modulates, and re-transmits the received signal, so that the complexity of a DF relaying node is significantly higher due to its additional processing capability. The spectrum sharing system restricts the maximum transmit power, P_T, at the

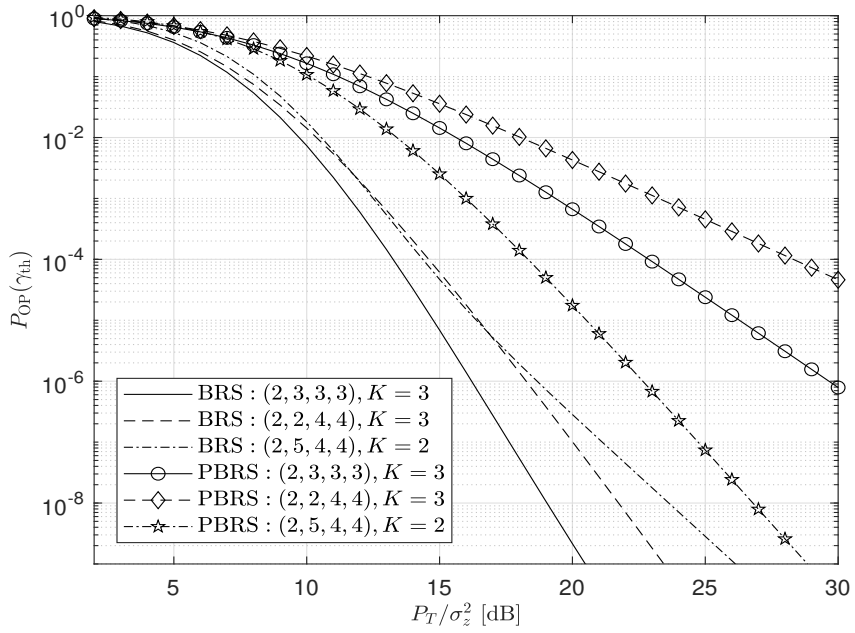

Fig. 17. Outage probability for various parameters. Two different relay selections are considered for comparisons. Elements of (N_1, N_2, N_3, N_4) respectively denote the number of multipath elements of $\boldsymbol{h}^{S\to j}$, $\boldsymbol{h}^{j\to D}$, $\boldsymbol{g}^{S\to PU}$, and $\boldsymbol{f}^{j\to PU}$.

SU-S and SU-R$_j, \forall j$, and the peak interference power at the PU, I_p. Under the constraint of χ_1, the transmit power at SU-S is given by $P_S = \frac{I_p}{\|\boldsymbol{g}^{s\to \mathrm{PU}}\|^2}$. The SNRs realized at SU-R$_j$ and SU-D via SU-R$_j$ are respectively given by $\lambda_{1,j} = \frac{P_S\|\boldsymbol{h}^{S\to j}\|^2}{\sigma_z^2}$ and $\lambda_{2,j} = \frac{P_R\|\boldsymbol{h}^{j\to D}\|^2}{\sigma_z^2}$, where $P_R = \frac{I_p}{\|\boldsymbol{f}^{j\to \mathrm{PU}}\|^2}$ is also limited by the constraint of χ_1. By BRS, the index of the selected relay node is determined by $j^*_{\mathrm{BRS}} = \arg\max_j \min(\lambda_{1,j}, \lambda_{2,j})$, whereas it will be determined by PBRS as follows: $j^*_{\mathrm{PBRS}} = \arg\max_j(\lambda_{1,j})$. Upon applying the relay selection scheme by either BRS or PBRS, the achievable SNRs by the DF relaying protocol are respectively given by $\gamma_{\mathrm{BRS}} \overset{\triangle}{=} \max\min(\gamma_{1,j^*_{\mathrm{BRS}}}, \gamma_{2,j^*_{\mathrm{BRS}}})$ and $\gamma_{\mathrm{PBRS}} \overset{\triangle}{=} \max\min(\gamma_{1,j^*_{\mathrm{PBRS}}}, \gamma_{2,j^*_{\mathrm{PBRS}}})$. Upon deriving these realized SNRs, the outage probability is used as the performance metric.

- Fig. 17 illustrates that a similar full diversity can be exploited by the SU network as that of the non-spectrum sharing CP-SC relaying system. That is, the full diversity can be seen as functions of multiuser diversity and multipath diversity either in the region of high interference power or maximum transmit power. For instance, from scenarios $((2,3,3,3), K=3)$ and $((2,2,4,4), K=3)$, we can show that the first two parameters determine the performance. Thus, scenario $((2,3,3,3), K=3)$ results in a lower outage probability compared with scenario $((2,3,3,3), K=3)$ at the same K, that is, at the same multiuser diversity. From scenarios $((2,3,3,3), K=3)$ and $((2,5,4,4), K=2)$, we can show that $K=3$ results in a lower outage probability due to a greater multiuser diversity. Hence, it can be verified that multipath diversity and multiuser diversity

jointly determine the total diversity. When we compare the outage probability in terms of relay selection by either BRS or PBRS, notice that BRS results a lower outage probability for all the considered scenarios. In addition, by using spectrum sharing and multiple relaying nodes in frequency selective fading channels, a greater diversity gain can be exploited compared with the other spectrum sharing systems that achieve only multiuser diversity.

- In summary, by integrating CP-SC transmissions with QRD-M-based data detection, high-reliable spectrum accessing capability can be achieved by the SU network.

We can also employ the DF relaying protocol and selection combining (SeC) [30] to increase the spectrum accessing capability, and verified that when the interference is proportional to the limited transmission power, the achievable outage diversity is equal to the diversity for the system with an unlimited transmission power.

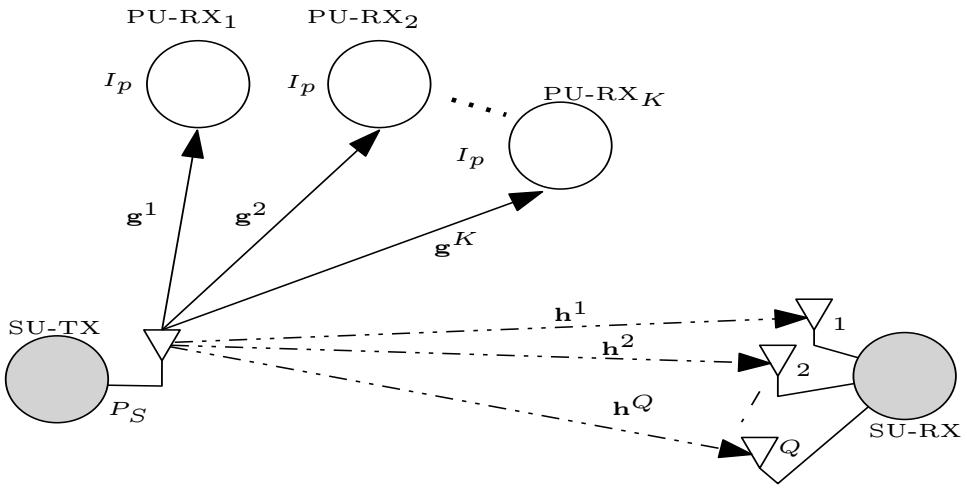

Fig. 18. Illustration of the CP-SC spectrum sharing system in the presence of K PU receivers.

For the spectrum sharing system illustrated in Fig. 18, we can apply CP-SC transmissions in the presence of multiple PU receivers and QRD-M-based data detection at every node.

- The SU-TX and PU-RXs are assumed to have a single antenna, whereas the SU-RX is assumed to have Q antennas. Maximal-ratio combining (MRC) and SeC are considered at the SU-RX.
- The peak interference power at all the PUs is assumed to be I_p. CP-SC transmissions are used in the considered spectrum sharing system, so that the transmit power at the SU-TX is given by $P_S = \min(P_T, \frac{I_p}{\max_k \|\boldsymbol{g}^k\|^2})$ constrained by χ_1 and χ_2. The number of multipath elements of $\boldsymbol{h}^q, \forall q$, is assumed to be N_h. The received signal at the qth antenna of the SU-RX is given by $\boldsymbol{y}^q = \sqrt{P_S}\boldsymbol{H}^q\boldsymbol{x} + \boldsymbol{z}$, where $\boldsymbol{H}^q$ is the right circulant matrix determined by $\boldsymbol{h}^q$ by CP-SC transmissions. Thus, the realized SNR at the SU-RX via the qth antenna is given by $\gamma^q \triangleq \frac{P_S\|\boldsymbol{h}^q\|^2}{\sigma_z^2} \triangleq \rho\|\boldsymbol{h}^q\|^2$, with $\rho \triangleq \frac{P_S}{\sigma_z^2}$, and then the SNR achieved by MRC and QRD-M-based data

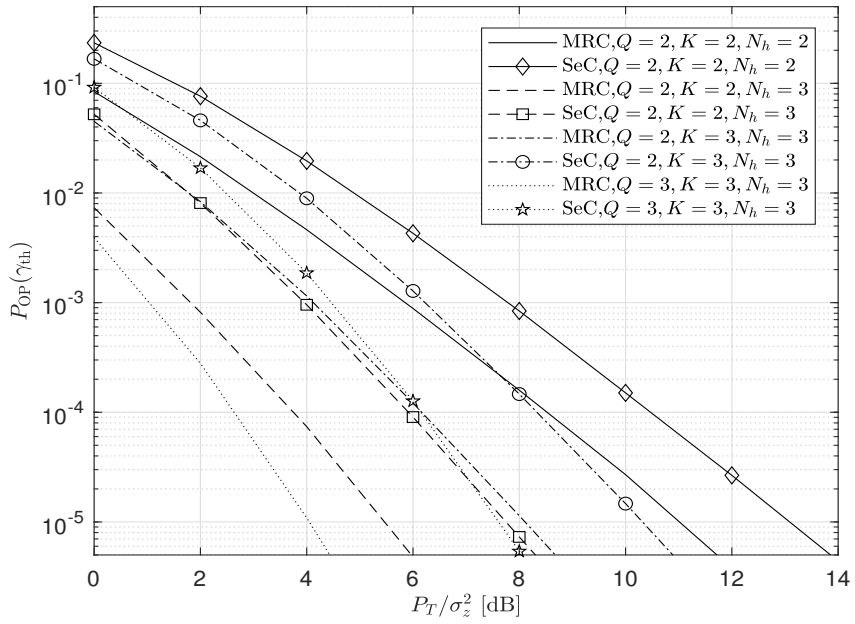

Fig. 19. Outage probability of the spectrum sharing system for various parameters. K PU receivers are assumed in the system.

detection is given by $\gamma \stackrel{\triangle}{=} \sum_{q=1}^{Q} \gamma^q = \rho \sum_{q=1}^{Q} \sum_{j=0}^{N_h-1} |h_{q,j}|^2$, where $h_{q,j}$ denotes the jth element of $\boldsymbol{h}^q$. For the realized SNR at the RX, the outage probability is used as the performance metric. In contrast, the realized SNR by SeC is given by $\gamma_{\rm SeC} = \rho \max_q (\sum_{j=0}^{N_h-1} |h_{q,j}|^2)$. Thus, in general, $\gamma_{\rm SeC} < \gamma$, which results in a worse performance than MRC-based operation.

- With various combinations of (Q, K, N_h), Fig. 19, which is showing the outage probability, verifies that as either N_h, the number of multipath elements of the SU channel, or Q, the number of antennas at the SU-RX, increases, a lower outage probability is obtained by both combining protocols due to more powerful diversity, that is, eventually a higher spectrum accessing capability of the SU network. However, in general, MRC lowers the outage probability with respect to SeC since it can reduce the effects of asymmetric fading in the SU channels [76]. In addition, as M increases, a worse outage probability is obtained due to a more tight restriction in accessing licensed radio spectrum.
- In summary, the benefits are achievable from CP-SC transmissions that exploit multipath diversity and advanced receiver operation that employs MRC and QRD-M-based data detection to exploit further different types of diversity. In other words, a different type of the full diversity that jointly utilizes multipath diversity and receiver diversity is achieved by CP-SC transmissions.

The spectrum sharing system, illustrated in Fig. 20, is composed by multiple PU-TXs, PU-RXs, a single SU-TX,

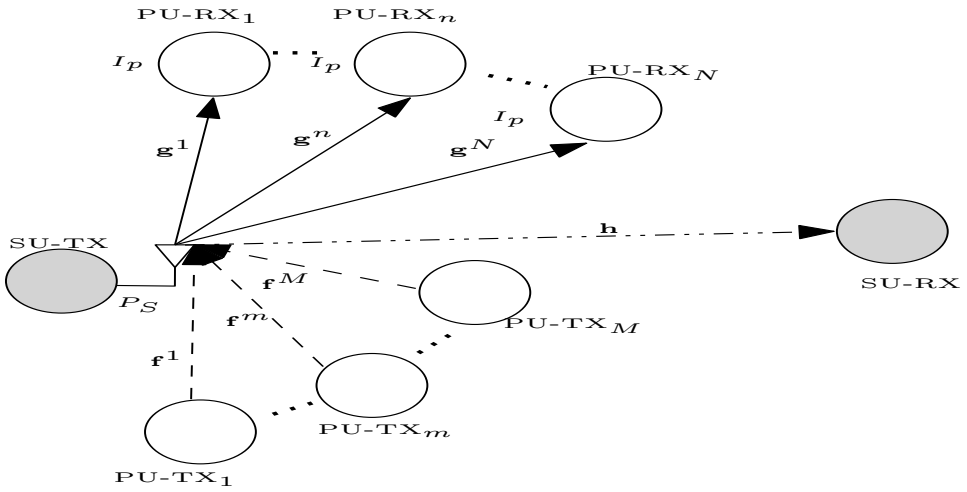

Fig. 20. Illustration of the spectrum sharing system in the presence of M PU transmitters and N PU receivers. All the nodes are assumed to be equipped with a single antenna. The sizes of $\boldsymbol{h}$, $\boldsymbol{g}^n$, and $\boldsymbol{f}^m$ are given by N_h, N_g, and N_f.

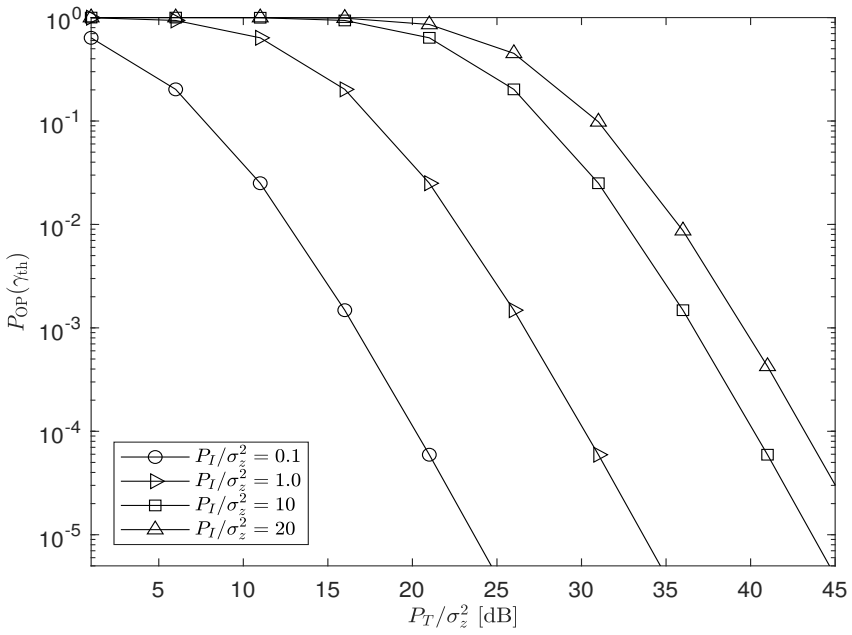

Fig. 21. Impact of interference power, P_I, on the outage probability.

and SU-RX, where both a single SU-TX and SU-RX forms the SU network.

- Due to the presence of multiple PU-TXs, interference from them will be another barrier to access radio spectrum by the SU network. Thus, it is an interesting problem to investigate their impact on the radio spectrum accessing

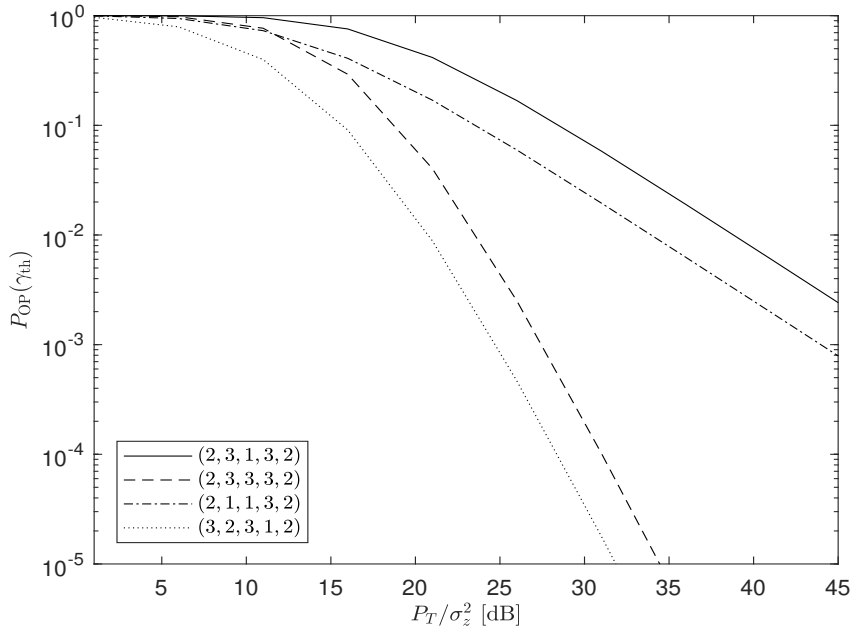

Fig. 22. The outage probability for various (M, N, N_h, N_f, N_g)s that specify system and channel parameters.

capability.

- According to constraints χ_1 and χ_2, the transmit power at the SU-TX is limited by $P_S = \min\left(P_T, \frac{I_p}{\max_n \|\boldsymbol{g}^n\|^2}\right)$, that is, it is restricted by the maximum transmit power, P_T, and the peak allowable interference at all the PU-RXs. The received signal at the SU-RX is given by $\boldsymbol{y} = \sqrt{P_s}\boldsymbol{H}\boldsymbol{x} + \sum_{p=1}^{M}\sqrt{P_{I_p}}\boldsymbol{F}^p\tilde{\boldsymbol{x}}_p + \boldsymbol{z}$, where $\boldsymbol{H}$ and $\{\boldsymbol{F}^p\}_{p=1}^M$ are right circulant matrices determined by the channels $\boldsymbol{h}$ and $\{\boldsymbol{f}^p\}_{p=1}^M$, P_{I_p} is the interference power from the pth PU-TX, and $\tilde{\boldsymbol{x}}_p$ is the interfering transmit block symbol satisfying $E\{\tilde{\boldsymbol{x}}_p\} = \boldsymbol{0}$ and $E\{\tilde{\boldsymbol{x}}_p(\tilde{\boldsymbol{x}}_p)^H\} = \boldsymbol{I}_Q,\ \forall p$. According to CP-SC transmissions, the realized SINR at the SU-RX is given by $\gamma_{\mathrm{SINR}} = \frac{P_S\|\boldsymbol{h}\|^2}{\sum_{p=1}^{Q} P_{I_p}\|\boldsymbol{f}^p\|^2+1}$. Then, the outage probability is given by $P_{\mathrm{OP}}(\gamma_{\mathrm{th}}) \triangleq Pr(\gamma_{\mathrm{SINR}} < \gamma_{\mathrm{th}})$ as a function of the SINR.
- For several values of interference power magnitude, Fig. 21 illustrates that the magnitude of interference power has no impact on the the outage probability. We assume that $M = 2$, $N = 2$, $N_h = 3$, and $N_f = 3$ for all the links from the PU-TXs to SU-RX, and $N_g = 2$ for all the links from the SU-TX to all the PU-RXs. In addition, Fig. 22 verifies that the exploitable diversity is mainly determined by N_h. Thus, the other system parameters, M and N, and channel parameters, N_f and N_g, have no impact on the exploitable diversity.

In summary, cooperative relaying schemes that employ CP-SC transmissions and QRD-M-based data detection have been effectively integrated into spectrum sharing systems with targeting at exploiting available different types of

diversity. In general, the more spectrum and better management inherently result in faster channel access, reduced interference and higher user throughput, and realizing massive IoT, IIoT, and 5G connectivity over unlicensed bands requires efficient and reliable spectrum sharing [61]. Thus, the use of CP-SC transmissions will be beneficial to establish reliable wireless system with allocated spectrum.

C. PLS Systems

In the wireless communication system, the transmission signal is propagated isotropically, so that its signal energy can be detected readily by legitimate and illegitimate users within the communication range of the transmitter regardless of the location of the users. Thus, protecting legitimate users from eavesdropping by illegitimate users is of critical interest of the wireless communication systems [77]. Due to the dynamic and large-scale topology, the key-based secure communication, which is usually implemented at the higher layers of the network stack, requires complex protocols for key management. In addition, the key distribution is a great challenge in its deployment [77]. In contrast, PLS uses the inherent randomness of wireless channels to achieve confidentiality of wireless communications. In general, PLS has the advantages of lowering the computational complexity and physical resource requirement, so that PLS is considered as a promising alternative to cryptography and has potential to protect the security of wireless communications. Many research efforts have been devoted to improving PLS with the aid of cooperative relaying [32], MIMO techniques [78], beamforming [79], and jamming [80]. In multiple antenna systems, beamforming is useful in increasing the link budget of the wireless link connecting with the legitimate user. For jamming based approaches, it is possible to improve PLS of the wireless network by degrading the SNR realized at the illegitimate user, while maintaining the desired SNR realized at the legitimate user with an acceptable minor SNR loss.

Ever since PLS was investigated for CP-SC transmissions by [32], many research activities have been accomplished [35], [81]. The emerging 5G system is characterized by a large scale of device connectivity in nature, so that it tends to be less robust to adversaries. From this reason, PLS is still an important research problem in protecting the communications from interception by illegitimate users and devices. We will introduce how CP-SC transmissions can be used to enhance PLS in the sequel.

We can exemplify the cooperative PLS system, which is illustrated in Fig. 23 [32]. It is composed by the source, S, K relaying nodes, $\{R_k\}_{k=1}^{K}$, Q destination nodes, $\{D_q\}_{q=1}^{Q}$, and N eavesdroppers, $\{D_n\}_{n=1}^{N}$. The DF relaying protocol with an assumption of perfect decoding at the relaying nodes is used.

- The frequency fading channels are assumed in the system, where sizes of $\boldsymbol{g}^{k,q}, \forall k, q$, and $\boldsymbol{h}^{k,j}, \forall k, j$, are given by N_1 and N_2. In addition, every node is equipped with a single antenna.
- Realized SNRs at R_k and E_n are respective given by $\gamma_1^{k,q}$ and $\gamma_2^{k,n}$, that is, $\gamma_1^{k,q} = \frac{P_s \|\boldsymbol{g}^{k,q}\|^2}{\sigma_z^2}$ and $\gamma_2^{k,n} = \frac{P_s \|\boldsymbol{h}^{k,n}\|^2}{\sigma_z^2}$. The transmission power at the relaying node is P_s, without applying constraints χ_1 and χ_2.

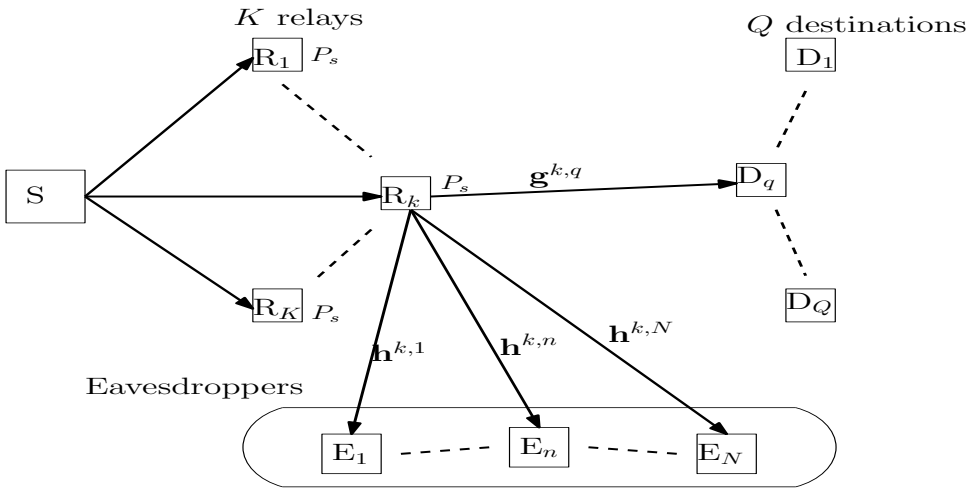

Fig. 23. Illustration of the cooperative PLS system with CP-SC transmissions.

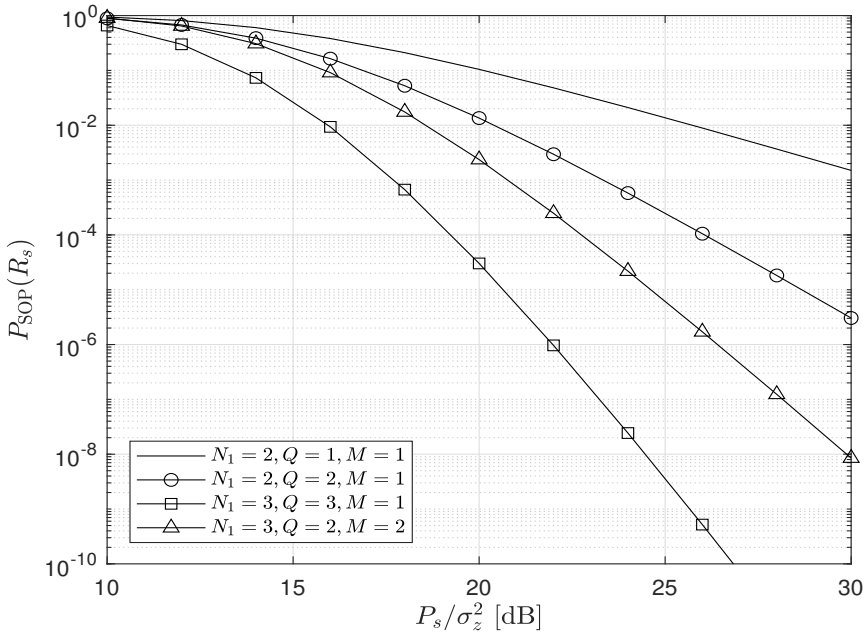

Fig. 24. Performance analysis: SOP.

- In the presence of a group of eavesdroppers, we can develop a selection mechanism for the relay and destination In particular, we can apply the two-stage relay and destination selection mechanism, which is some similar to the opportunistic user selection which is described in Section II-B-(5). To minimize the worst-case interception by the eavesdropper group, we first select one relay, i.e., R_k. Then, one desired destination, D_q, is selected

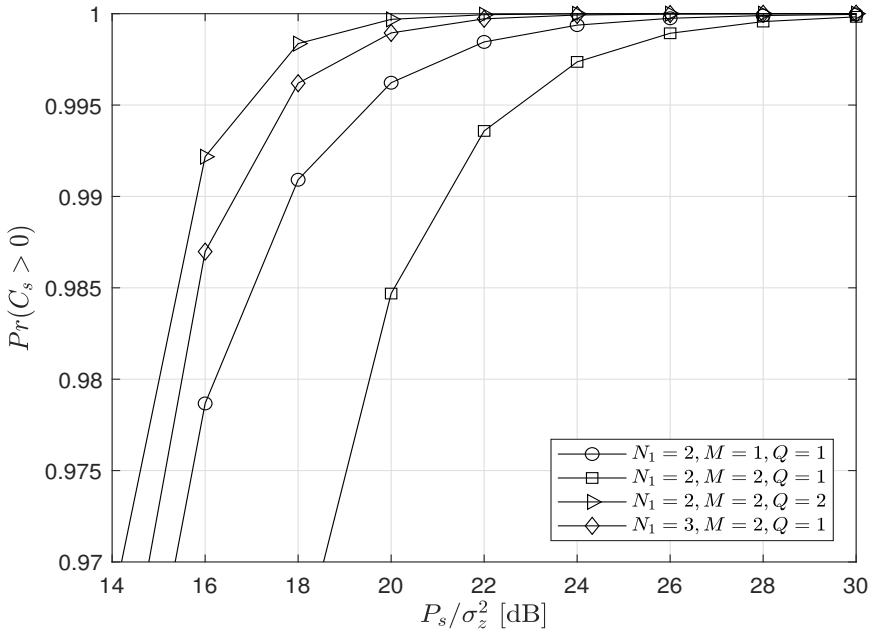

Fig. 25. Performance analysis: Probability of non-zero achievable secrecy rate.

by R_k to maximize the instantaneous SNR between them. Thus, the two-stage relay and destination selection mechanism can be expressed as follows:

$$\begin{aligned} \text{stage1} \quad &: \quad k^* = \min \arg_{k\in[1,K]}(\gamma_2^{k,\max}) \text{ and} \\ \text{stage2} \quad &: \quad q^* = \max \arg_{q\in[1,Q]}(\gamma_1^{k^*,q}) \end{aligned} \tag{13}$$

where $\gamma_2^{k,\max}$ and $\gamma_1^{k^*,q}$ respectively denote the maximum instantaneous SNR among those of between the kth relay and N eavesdroppers, and the maximum instantaneous SNR between the selected relay and the qth destination. Based on the realized SNRs, the instantaneous secrecy rate is given by $C_s = \frac{1}{2}[\log_2(1 + \gamma_1^{k^*,q^*}) - \log_2(1 + \gamma_2^{\min,\max})]^+$, where $\log_2(1 + \gamma_1^{k^*,q^*})$ is the instantaneous capacity of the channel between R_k and the selected destination. In addition, $\log_2(1 + \gamma_2^{\min,\max})$ is the instantaneous interception capacity by the intercepting channel between R_k and a set of eavesdroppers. With respect to the instantaneous secrecy rate, the SOP is used as the performance metric.

- The exploitable full diversity is determined by QN_1, which is verified by Fig. 24. A fixed $N_2 = 2$ and $P_s/\sigma_z^2 = 5$ dB is assumed. Thus, multipath diversity and multiuser diversity jointly affect the convergence speed of the non-zero achievable secrecy rate, which is verified by Fig. 25, where a fixed $N_2 = 3$ and $P_s/\sigma_z^2 = 5$ dB is assumed. The use of multiple antennas, employed in the form of MRC at each eavesdropper, does not affect secrecy diversity, which is verified by Fig. 24.

In summary, the cooperative CP-SC transmissions can exploit multipath and multiuser diversity in the considered channel environment to increase PLS. To achieve these diversities, QRD-M-based data detection and opportunistic user selection are necessary for the relays and destination nodes. Furthermore, the advanced eavesdropper will utilize QRD-M-based data detection to increase its interception capability. Since the full diversity is determined by the legitimate channels characteristics, the advanced receiver processing at the eavesdroppers does not impact on it.

D. dCDD-based Systems

The most unique features of dCDD are summarized as follows:

- Full CSI is not required at the transmitting side. Thus, dCDD can reduce a feeding overhead from the receiving side.
- Depending on the size of a block symbol, $\boldsymbol{s}$, and the maximum number of multipath components over the target channels, a set of desired RRHs can be selected by the CU in contrast to CDD, which is applicable to the set of transmit antennas installed at the single transmitter. Since dCDD always includes $\mathrm{RRH}_{(1)}$ that results in the greatest signal power at the RX, the full diversity can be exploited for under-populated and over-populated systems, which implicitly includes multiuser diversity.
- dCDD is adaptable to burst transmissions.

To exploit transmit diversity, dCDD has been applied to the following wide range of applications: General cooperative systems [82], [83]; spectrum sharing systems [29], [84], [85]; and PLS systems [35], [81]. In the sequel, we will introduce dCDD-based spectrum sharing system and dCDD-based PLS system for the further extension of CP-SC transmissions.

1) dCDD-Based Underlay Spectrum Sharing Systems: To effectively access radio spectrum, licensed to the PU, we can exemplify one dCDD-based cooperative system [29], which is illustrated in Fig.26. It is composed of the CU and M RRHs. Within the operation area of the SU-RX, we assume that one PU-RX, Q PU-TXs, and one SU-RX co-exist. For this new system setting, dCDD was utilized to increase the radio spectrum accessing capability.

- Under constraints of χ_1 and χ_2, the transmission power at SU-RRHs is given by $P_s = \min(P_T, \frac{I_p}{\max_m \|\boldsymbol{g}^m\|^2})$, where P_T and I_p are respectively maximum allowable transmission power at SU-RRHs and the peak allowable interference at the PU-RX.
- The received signal at SU-RX is given by $\boldsymbol{y} = \sqrt{P_s}\boldsymbol{H}_{\mathrm{dCDD}}\boldsymbol{x} + \sqrt{P_p}\sum_{q=1}^{Q}\boldsymbol{F}_q\boldsymbol{x}_q + \boldsymbol{z}$, where $\boldsymbol{H}_{\mathrm{dCDD}}$ and $\{\boldsymbol{F}_q\}_{q=1}^{Q}$ are right circulant matrices respectively determined by $\{\boldsymbol{h}^m\}_{m=1}^{M}$ and $\{\boldsymbol{f}^q\}_{q=1}^{Q}$, and P_p is the transmission power at the PU-TXs. An interfering block symbol from the qth PU-TX is denoted by $\boldsymbol{x}_q$. Refer to Section II-B-(6) in obtaining an equivalent channel matrix $\boldsymbol{H}_{\mathrm{dCDD}}$ by dCDD. When we assume statistical un-correlation among the desired transmission symbol block and interfering symbol blocks, then the SIR is given by $\gamma =$

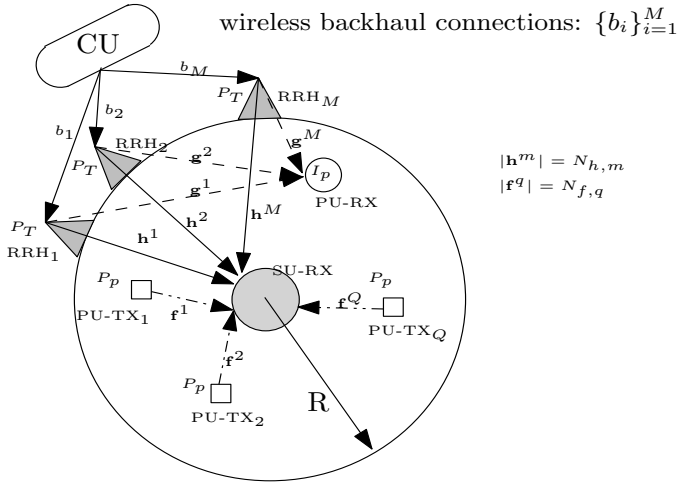

Fig. 26. Illustration of the dCDD-based spectrum sharing system with the CU and M RRHs.

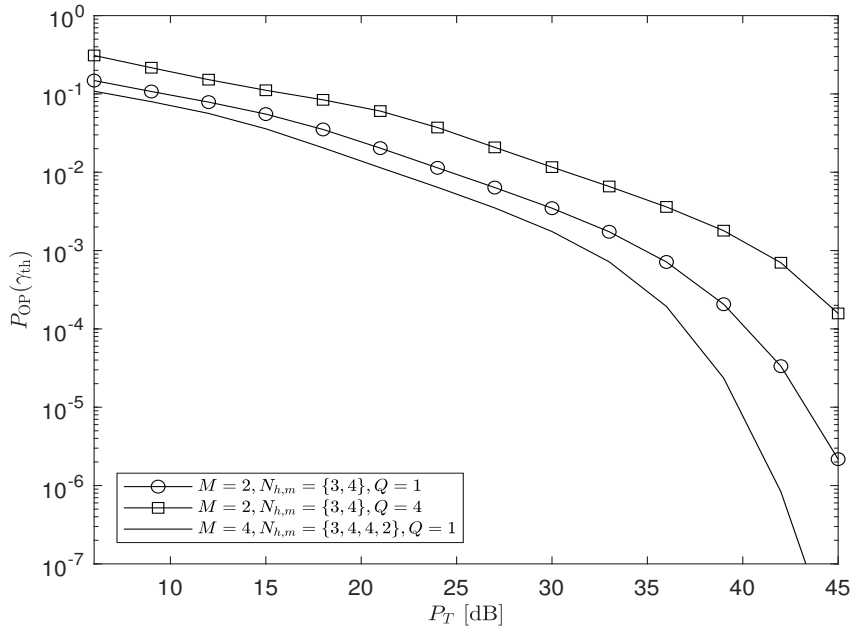

Fig. 27. Outage probability of the secondary network of dCDD-based spectrum sharing system.

$\frac{P_s \sum_{m=1}^{M} \|\boldsymbol{h}^m\|^2}{P_p \sum_{q=1}^{Q} \|\boldsymbol{f}^q\|^2}$, which illustrates that the signal power is more aggregated at the RX under the same interference condition. Using the realized SIR, the outage probability is used as the performance metric.

- Fig. 27 illustrates the benefits of dCDD in accessing spectrum. We assume two multipath components over the channels from PU-TXs to SU-RX and from RRHs to PU-RX, that is, $N_{h,m} = N_{f,q} = 2, \forall m, q$. We can

see that as more RRHs are supported by dCDD, dCDD can lower the outage probability.

- In summary, in contrast to transmit antenna selection (TAS), dCDD-based spectrum sharing systems can reduce the feeding back overhead and remove the requirement of full CSI at the CU and RRHs. Thus, the dCDD-based transmit diversity or macro diversity scheme is a practical solution to handle scarce radio spectrum and to increase the spectrum accessing capability with supporting the full diversity.

2) dCDD-Based PLS Systems: We can exemplify one CP-SC system that employs dCDD [35] to increase PLS by virtue of transmit diversity.

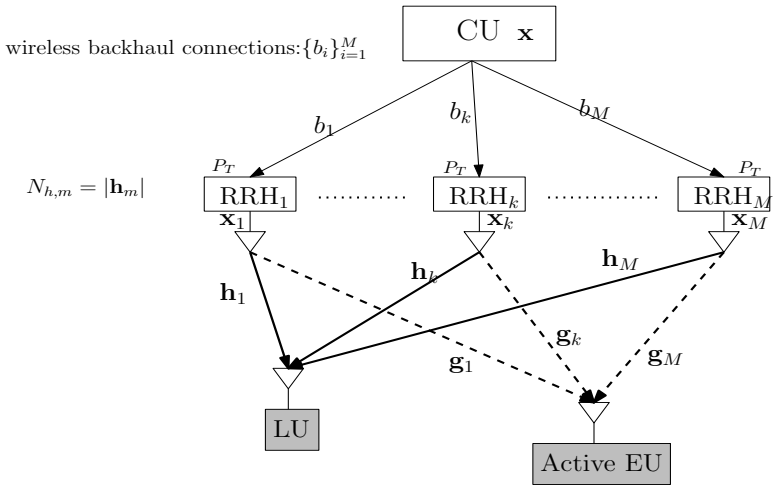

Fig. 28. Illustration of the dCDD-based cooperative system with PLS in the presence of one active EU.

For the system illustrated in Fig. 28, one of the RRHs is chosen to be working as an interfering RRH that transmits a deliberately interfering signal to the active legitimate user (LU) and eavesdropping user (EU), in a way that a RRH that results in the greatest channel strength at the EU is selected as the interfering RRH.

- Under the assumption that the CU has the knowledge of the channels from RRHs to active EU, then it sorts the channels in terms of their magnitude as: $\|\boldsymbol{g}_{(1)}\|^2 \leq \cdots \leq \|\boldsymbol{g}_{(M)}\|^2$. Then, the interfering RRH, indexed by (M), is chosen as the interfering RRH, while the remaining $M-1$ RRHs are selected as the transmit RRHs that transmit the desired block symbol to LU.
- After the removal of the CP signal with CP-SC transmissions, the received signal at LU is given by $\boldsymbol{y}_L = \sqrt{P_T}\sum_{l=1,l\neq(M)}^{M}\boldsymbol{H}_m\boldsymbol{P}_{\Delta_m}\boldsymbol{x} + \sqrt{P_T}\boldsymbol{H}_{(M)}\boldsymbol{P}_{\Delta_{(M)}}\boldsymbol{j} + \boldsymbol{z}$, where $\{\boldsymbol{H}_m\}_{m=1,m\neq(M)}^{M}$ and $\boldsymbol{H}_{(M)}$ are right circulant matrices, and $\boldsymbol{j}$ is the interfering signal generated by a Zadoff-Chu sequence. Since the null space of an equivalent channel matrix does not exist, we can use the Zadoff-Chu sequence as the AN sequence. Referring to Section II-B-(6), $\{\boldsymbol{P}_{\Delta_m}\}_{m=1,m\neq(M)}^{M}$ and $\boldsymbol{P}_{\Delta_{(M)}}$ transform the block symbol, $\boldsymbol{x}$, to $\boldsymbol{x}_k$, which is the circularly shifted version of $\boldsymbol{x}$. Perfect wireless backhaul connections, $\{b_1, \ldots, b_K\}$, are considered in the system. Since

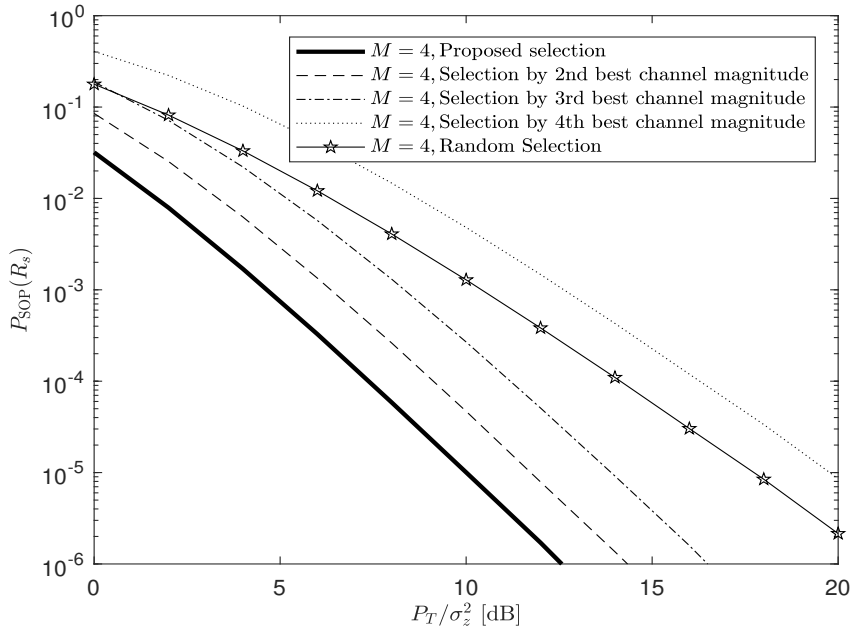

Fig. 29. SOP with different types of interfering RRH selection schemes.

the interfering signal is only known to LU, the interfering signal can be removed for its receiver processing, so that the received signal can be formulated as $\boldsymbol{y}_L = \sqrt{P_T}\sum_{l=1,l\neq(M)}^{M}\boldsymbol{H}_m\boldsymbol{P}_{\Delta_m}\boldsymbol{x} + \boldsymbol{z}$.

- After the removal of the CP signal with CP-SC transmissions, the received signal at EU is given by $\boldsymbol{y}_E = \sqrt{P_T}\sum_{l=1,l\neq(M)}^{M}\boldsymbol{G}_m\boldsymbol{P}_{\Delta_m}\boldsymbol{x} + \sqrt{P_T}\boldsymbol{G}_{(M)}\boldsymbol{P}_{\Delta_{(M)}}\boldsymbol{j} + \boldsymbol{z}_E$, where $\{\boldsymbol{G}_m\}_{m=1,m\neq(M)}^{M}$ and $\boldsymbol{G}_{(M)}$ are right circulant matrices. In contrast to the signal reception at LU, there are two possibilities to protect from eavesdropping: i) When EU has no knowledge of the AN, it is not easy to remove the interfering signal in its receiving process; and ii) Since the permutation shifting matrices, $\{\boldsymbol{P}_{\Delta_m}\}_{m=1,m\neq(M)}^{M}$ and $\boldsymbol{P}_{\Delta_{(M)}}$ are mainly determined by the legitimate channels from M RRHs to RX, $\{\boldsymbol{h}_m\}_{m=1}^{M}$, these permutation shifting matrices are not perfect in removing ISI when EU applies dCDD to increase its interception capability.
- From received signals at LU and EU, the realized SNR at the LU is given by $\gamma_L = \rho\sum_{l=1,l\neq(M)}^{M}\|\boldsymbol{h}_m\|^2$, whereas the realized SINR at EU is given by $\gamma_E = \frac{P_T\sum_{l=1,l\neq(M)}^{M}\|\boldsymbol{g}_m\|^2}{P_J\|\boldsymbol{g}_{(M)}\|^2+\sigma_z^2}$ under the condition that $N_{\mathrm{CP}} = \max(\{N_{h,m}\}_{m=1}^{M})$ over $\{\boldsymbol{h}_m\}_{m=1}^{M}$, is same as that of the illegitimate channels, $\{\boldsymbol{g}_m\}_{m=1}^{M}$.
- The transmission capacity achieved by the legitimate CP-SC transmissions is given by $C_L = \log_2(1+\gamma_L)$, whereas the interceptable capacity is given by $C_E = \log_2(1+\gamma_E)$, so that the secrecy capacity is given by $C_s = [C_L - C_E]^+$. At a given secrecy rate, R_s, the SOP is used as the performance metric.
- Fig. 29 illustrates that the proposed selection scheme is the best in degrading the SNR at the EU, so that it

can reduce information leakage at the EU.

IV. Future Directions

A. Spectrum Sharing in Future Cooperative CP-SC Transmissions

- To increase system throughput and peak data rate of wireless systems, it is necessary to aggregate a plurality of distributed frequency bands under the constraint of bounded latency. However, available bands are limited, so that new smart band aggregation is required to be incorporated with the spectrum sharing. In particular, TVWS, licensed frequency bands, unlicensed high frequency bands such as mmWave and Tera-Hertz bands can be considered for spectrum aggregation (SA) [61], [86], [87]. Thus, depending on the operating frequency, coverage, and service requirement, smart spectrum management is necessary to handle various types of frequency bands before applying the spectrum sharing (SS).
- When both PU and SU leverage unlicensed bands, how to satisfy predictable and guaranteed QoS levels is challenging over the unlicensed bands since transmissions on unlicensed spectrum are not reliable. How to handle coexistence is another issue since multiple unlicensed and licensed users can coexist in the same frequency bands. In addition, interference from other frequency bands and malicious jamming will be intrinsic problems that can result in service discontinuity. Thus, a new agile and robust SS scheme to effectively use the unlicensed bands with guaranteed QoS will be necessary. Furthermore, an interference control mechanism is required to be incorporated to develop a robust SS scheme.
- Although this paper considers a distributed system composed of multiple nodes, how to make SS support numerous connected nodes and ensure high data rates for concurrently connected nodes, is another problem, which is a typical use case of 5G and B5G.
- Although SS can reduce the spectrum sensing requirement, another issue is how to provide guaranteed QoS with mobile users. Thus, the development of a dynamic SS with a DSA is an important problem.
- Distributed machine learning and reinforcement learning in the SU can be used to make intelligent decisions regarding access of the frequency band without harming the PU.

B. Cooperative Relaying in Future Cooperative CP-SC Transmissions

- The CP-SC transmission may be a good choice for cooperative relaying scenarios where a relay has its own information of a low data rate to transmit in addition to forwarding the information of the source that has a relatively high date rate, e.g., the relay can be a sensor and needs to report the sensed data to the destination.
- The implementation can be diverse depending on the number of relays and whether there is a central unit to control the relays in the presence of more than one relay. Specifically, for the case of only one relay, after decoding the CP-SC signal sent by the source, the relay can encode its own information onto the cyclic

delay value of the forwarded CP-SC signal. As long as the cyclic delay is chosen to be nonzero, a CDD gain is attainable when the destination combines the received signals from the source and relay. For the case of multiple relays, if the relays can be controlled by a central unit, the sensed data can be encoded onto the permutation of different cyclic delay values each adopted by a different relay. A maximum CDD gain can be obtained after combining all received signals at the destination when the cyclic delay values are chosen in such a way that the channel taps from all relays to the destination are separated without any overlap in the delay domain. Clearly, in both cases the source and relay become symbiotic. However, when there is not a central unit, all relays are not aware of the cyclic delay values employed by the other relays so that a perfect separation of channel taps may not always be guaranteed. How to harvest the maximum CDD gain is thereby challenging, which requires further study.

C. PLS in Future Cooperative CP-SC Transmissions

- Smart wireless propagation is enabled by reconfigurable intelligence surfaces (RISs), which provide an additional method to prevent illegitimate users from eavesdropping upon legitimate transmissions. Through passive beamforming, an RIS can reduce reflected signal power in the direction of the illegitimate user while maintaining the signal power in the direction of the legitimate user. When using CP-SC transmissions, the RIS's passive beamforming design must account for the wideband signal processing issues in either TD or FD. In addition, the active RIS can improve the PLS performance for CP-SC transmissions by increasing the reflecting amplitude while maintaining an energy efficiency comparable to that of a RIS.
- To further enhance the PLS performance, multiple RISs can be deployed to provide spatial diversity in CP-SC transmissions, which results in more complicated optimization problems than those in narrowband transmissions.
- In the next generation of multiple access systems, CP-SC transmissions will interplay with various multiple access schemes including NOMA, rate splitting multiple access, random access, grant-free and semi-grant-free access. To ensure the PLS performance of a specific multiple access system using CP-SC transmissions, waveform design, transceiver design and PLS schemes need to be jointly optimized subject to the specific ultra-low latency and ultra-reliability constraints, which are more stringent than the QoS requirements of existing communication systems.
- Although the CP can provide diversity gain for CP-SC transmissions, which is beneficial to enhance the PLS performance, it also introduces an additional time delay, which is undesirable in short packet transmissions. Thus, how to trade-off between the PLS performance and the stringent QoS requirements is still an open problem for CP-SC transmissions in the next generation of multiple access systems.

D. CDD/dCDD in Future Cooperative CP-SC Transmissions

- Although non-orthogonal multiple access (NOMA) has been widely exploited in many areas, the use of dCDD in NOMA is still in the early stage. One recent application is provided by the work of [88] that divides a set of RRHs into two groups to support two users simultaneously with different symbol blocks, $\boldsymbol{x}_1$ and $\boldsymbol{x}_2$ to the far user and near user, respectively. To maximize the rate of the far user and the sum rate of two users under a near-far user pairing constraint, an efficient RRH selection is developed. Some of the open questions are as follows: i) how to handle more than two users under two constraints of dCDD with CP-SC transmissions; ii) how to support multi-clusters composed of at least two users; and iii) how to employ CP-SC transmissions in uplink transmissions. Since dCDD-based NOMA can exploit the full diversity in the frequency selective fading channel to improve its throughput, we expect further researches in this area.
- Built on 5G technologies, a private 5G network [61] is a dedicated network that supports many industrial applications in different vertical sectors by accommodating and processing the information gathered through a large number of sensors, actuators, and robots. Techniques harvesting spatial diversity are one of the key techniques to simultaneously achieve low latency and high reliability. When the network increases the number of distributed nodes/devices to achieve spatial diversity, interference will be increased. Furthermore, time synchronization among distributed nodes/devices will be challenging and additional feedback overhead will be increased. One recent employment of dCDD in the private 5G network is provided by [89] that proposes the multi-cluster-based dCDD to improve coverage over a large network area and to increase channel diversity. When each node is recognized as the BS, dCDD can be recognized as a CoMP, which was shown to be very effective in achieving low-latency and high-reliability in industrial automation [90]. Although many heterogeneous nodes/devices are expected in private sectors, their behaviors in a particular private sector will be statistically consistent and unique. Thus, how to integrate local statistics into CP-SC transmissions is open problem that deserves further study.
- Estimating all the reflected multipath channels within the coherence time is very challenging for reconfigurable intelligent surface (RIS) empowered broadband wireless systems. Even though a channel estimation issue can be resolved, how to constructively combine all the independently reflected mutipath signals from the RIS elements to harvest a significant diversity gain remains a second challenging issue. OFDM signaling has been shown to be an efficient method to estimate the channels in the FD, but the subcarrier-wise passive beamforming fails to attain the full multipath diversity. The CP-SC transmission provides a clever solution to both challenging issues mentioned above. The idea is to create different cyclically delayed versions of the incident signal by configuring the RIS according to the transmitted PSK symbols such that all reflected multipath signals from the RIS elements can be perfectly resolvable in the TD, as similar to the CDD technique. In this way, all the multipath signals in the TD can be easily obtained via a simple decorrelation operation when a cyclic orthogonal

training sequence is employed and full multipath diversity can be harvested by MMSE equalization.

V. Conclusions

This paper has surveyed recent research on CP-SC transmissions-based cooperative and distributed systems. After having introduced the basic principle of CP-SC transmissions, we have demonstrated that exploiting full diversity is the key merit of CP-SC transmissions for cooperative and distributed systems. By virtue of full diversity, we have verified that high reliability can be achieved in the environment with frequency selective fading channels. Finally, we have identified some future directions for CP-SC transmissions.

References

[1] *Digital Video Broadcasting (DVB). Frame Structure Channel Coding and Modulation for a Second Generation Digital Terrestrial Television Broadcasting System (DVB-T2)*, DVB-T2 Std. ETSI EN 302 755 V1.3.1l, 2012.

[2] *Radio Broadcasting Systems; Digital Audio Broadcasting (DAB) to mobile, portable and fixed receivers*, DAB Std. EN 300 401 V2.1.1, Oct. 2016.

[3] *Wireless Medium Access Control (MAC) and Physical Layer (PHY) Specifications for High Rate Wireless Personal Area Networks (WPANs): Amendment 2: Millimeter-wave based Alternative Physical Layer Extension*, IEEE Std. 802.15.3c, Sep. 2009.

[4] *Wireless LAN Medium Access Control (MAC) and Physical Layer (PHY) Specifications - Amendment 5: Enhancements for Higher Throughput*, IEEE Std. 802:11n, Mar. 2012.

[5] *Wireless LAN Medium Access Control (MAC) and Physical Layer (PHY) Specifications–Amendment 4: Enhancements for Very High Throughput for Operation in Bands below 6 GHz*, IEEE Std. 802.11ac, 2013.

[6] *Wireless LAN Medium Access Control (MAC) and Physical Layer (PHY) Specifications: Enhancements for Very High Throughput in the 60GHz Band*, IEEE Std. 802.11ad, Mar. 2012.

[7] *Wireless LAN Medium Access Control (MAC) and Physical Layer (PHY) Specifications–Amendment: Enhanced Throughput for Operation in License-Exempt Bands Above 45 GHz*, IEEE Std. 802.11ay, Jun. 2019.

[8] *IEEE Standard for Broadband over Power Line Networks: Medium Access Control and Physical Layer Specifications – Amendment 1: Enhancement for Internet of Things Applications*, IEEE Std. 1901, 2010.

[9] D. Castelain, C. Ciochina-Duchesne, J. Guillet, and F. Hasegawa, "SC-OFDM, a low complexity technique for high performance satellite communications," in *32nd AIAA Int. Commun. Satellite Systems Conf.*, San Diego, CA, Aug. 2014, pp. 1–8.

[10] Y. Rahmatallah and S. Mohan, "Peak-to-average power ratio reduction in OFDM systems: A survey and taxonomy," *IEEE Commun. Surveys Tuts.*, vol. 15, no. 4, pp. 1567–1592, Fourth quarter 2013.

[11] S. H. Han and J. H. Lee, "An overview of peak-to-average power ratio reduction techniques for multicarrier transmission," *IEEE Wireless Commun.*, vol. 12, pp. 56–65, Apr. 2005.

[12] H. Wang, P. M. Asbeck, and C. Fager, "Millimeter-wave power amplifier integrated circuits for high dynamic range signals," *IEEE J. Microwaves*, vol. 1, no. 1, pp. 299–316, Winter 2021.

[13] S. Sesia, I. Toufik, and M. Baker, *LTE -The UMTS Long Term Evolution From Theory to Practice*. West Sussex, United Kingdom: John Wiley and Sons Ltd, 2009.

[14] A. Barbieri, G. Colavolpe, T. Foggi, E. Forestieri, and G. Prati, "OFDM versus single-carrier transmission for 100 Gbps optical communication," *J. Lightw. Technol.*, vol. 28, no. 17, pp. 2537–2551, Sep. 2010.

[15] Y. Wang and X. Dong, "Comparison of frequency offset and timing offset effects on the performance of SC-FDE and OFDM over UWB channels," *IEEE Trans. Veh. Technol.*, vol. 58, no. 1, pp. 242–250, Jan. 2009.

[16] C. He *et al.*, "Time-frequency domain Turbo equalization for single-carrier underwater acoustic communications," *IEEE Access*, vol. 7, pp. 73 324–73 335, 2019.

[17] Y. H. Ng and T. C. Chuah, "Single-carrier cyclic prefix-assisted PLC systems with frequency-domain equalization for high-data-rate transmission," *IEEE Trans. Power Del.*, vol. 25, no. 3, pp. 1450–1457, Jul. 2010.

[18] H. G. Myung and D. J. Goodman, *Single Carrier FDMA: A New Air Interface for Long Term Evolution*, 1st ed. West Sussex, United Kingdom: John Wiley and Sons, 2008.

[19] Y. Wang, X. Dong, P. H. Wittke, and S. Mo, "Cyclic prefixed single carrier transmission in ultra-wideband communications," *IEEE Trans. Wireless Commun.*, vol. 5, no. 8, pp. 2017–2021, Aug. 2006.

[20] K. J. Kim and T. A. Tsiftsis, "Performance analysis of QRD-based cyclically prefixed single-carrier transmissions with opportunistic scheduling," *IEEE Trans. Veh. Technol.*, vol. 60, no. 1, pp. 328–333, Jan. 2011.

[21] F. Schaich, T. Wild, and R. Ahmed, "Waveform contenders for 5G - suitability for short packet and low latency transmissions," in *Proc. 2014 IEEE Vehicular Technology Conference (VTC-Spring)*, Seoul, Korea, May. 2014, pp. 1–5.

[22] K. J. Kim, M. D. Renzo, H. Liu, P. V. Orlik, and H. V. Poor, "Performance analysis of distributed single carrier systems with distributed cyclic delay diversity," *IEEE Trans. Commun.*, vol. 65, no. 12, pp. 5514–5528, Dec. 2017.

[23] K. J. Kim, T. Q. Duong, H. V. Poor, and M. H. Lee, "Performance analysis of adaptive decode-and-forward cooperative single-carrier systems," *IEEE Trans. Veh. Technol.*, vol. 61, no. 7, pp. 3332–3337, Sep. 2012.

[24] H. Chergui, T. Ait-Idir, M. Benjillali, and S. Saoudi, "Joint-over-transmissions project and forward relaying for single carrier broadband MIMO ARQ systems," in *Proc. IEEE Veh. Techol. Conf.*, Yokohama, Japan, May 2011, pp. 1–5.

[25] Y. Deng *et al.*, "Full-duplex spectrum sharing in cooperative single carrier systems," *IEEE Trans. on Cogn. Commun. Netw.*, vol. 2, no. 1, pp. 68–82, Mar. 2016.

[26] K. J. Kim, T. A. Tsiftsis, and H. V. Poor, "Power allocation in cyclic prefixed single-carrier relaying systems," *IEEE Trans. Wireless Commun.*, vol. 10, no. 7, pp. 2297–2305, Jul. 2011.

[27] K. J. Kim, T. Q. Duong, H. V. Poor, and L. Shu, "Performance analysis of cyclic prefixed single-carrier spectrum sharing relay systems in primary user interference," *IEEE Trans. Signal Process.*, vol. 60, no. 12, pp. 6729–6734, Dec. 2012.

[28] K. J. Kim, T. Q. Duong, and H. V. Poor, "Performance analysis of cyclic prefixed single-carrier cognitive amplify-and-forward relay systems," *IEEE Trans. Wireless Commun.*, vol. 12, no. 1, pp. 195–205, Jan. 2013.

[29] K. J. Kim, H. Liu, M. Wen, M. D. Renzo, and H. V. Poor, "Outage probability analysis of spectrum sharing systems with distributed cyclic delay diversity," *IEEE Trans. Commun.*, vol. 67, no. 6, pp. 4435–4449, Jun. 2019.

[30] K. J. Kim, T. Q. Duong, and H. V. Poor, "Outage probability of single-carrier cooperative spectrum sharing systems with decode-and-forward relaying and selection combining," *IEEE Trans. Wireless Commun.*, vol. 12, no. 2, pp. 806–817, Feb. 2013.

[31] K. J. Kim, P. L. Yeoh, P. Orlik, and H. V. Poor, "Secrecy performance of finite-sized cooperative single carrier systems with unreliable backhaul connections," *IEEE Trans. Signal Process.*, vol. 64, no. 17, pp. 4403–4416, Sep. 2016.

[32] L. Wang, K. J. Kim, T. Q. Duong, M. Elkashlan, and H. V. Poor, "Security enhancement of cooperative single carrier systems," *IEEE Trans. Inf. Forensics Security*, vol. 10, no. 1, pp. 90–103, Jan. 2015.

[33] H. Liu, P. L. Yeoh, K. J. Kim, P. V. Orlik, and H. V. Poor, "Secrecy performance of finite-sized in-band selective relaying systems with unreliable backhaul and cooperative eavesdroppers," *IEEE J. Sel. Areas Commun.*, vol. 36, no. 7, pp. 1499–1516, Jul. 2018.

[34] K. J. Kim, J. Guo, J. Tang, and P. V. Orlik, "Distributed cyclic delay diversity for cooperative infrastructure-to-vehicle systems," in *Proc. 2019 IEEE GLOBECOM*, Taipei, Taiwan, Dec. 2019, pp. 1–6.

[35] K. J. Kim, H. Liu, M. D. Renzo, P. V. Orlik, and H. V. Poor, "Secrecy analysis of distributed CDD-based cooperative systems with deliberate interference," *IEEE Trans. Wireless Commun.*, vol. 12, no. 17, pp. 7865–7878, Dec. 2018.

[36] M. Levesque and D. Tipper, "A survey of clock synchronization over packet-switched networks," *IEEE Commun. Surveys Tuts.*, vol. 18, no. 4, pp. 2926–2947, Fourth quarter 2016.

[37] A. Nasrallah *et al.*, "Ultra-Low Latency (ULL) Networks: The IEEE TSN and IETF DetNet Standards and Related 5G ULL Research," *IEEE Commun. Surveys Tuts.*, vol. 21, no. 1, pp. 88–145, 1st Quarter 2019.

[38] J. M. Hamamreh, Z. E. Ankarali, and H. Arslan, "CP-less OFDM with alignment signals for enhancing spectral efficiency, reducing latency, and improving PHY security of 5G services," *IEEE Access*, vol. 6, pp. 63 649–63 663, 2018.

[39] B. Devillers and L. Vandendorpe, "Bit rate comparison of adaptive OFDM and cyclic prefixed single-carrier with DFE," *IEEE Commun. Lett.*, vol. 13, no. 11, pp. 838–840, Nov. 2009.

[40] Y. R. Zheng, J. Wu, and C. Xiao, "Turbo equalization for single-carrier underwater acoustic communications," *IEEE Commun. Mag.*, vol. 11, no. 53, pp. 79–87, Nov. 2015.

[41] P. J. David, *Circulant Matrices*. New York, NY: John Wiley and Sons, 1979.

[42] J. Jia, S. Wang, and K. Lai, "Hybrid-domain sequence detector for training sequence-aided single-carrier block transmission signals," *IEEE Trans. Wireless Commun.*, vol. 14, no. 12, pp. 6565–6578, Dec. 2015.

[43] S. G. Larew, T. A. Thomas, M. Cudak, and A. Ghosh, "Air interface design and ray tracing study for 5G millimeter wave communications," in *Proc. 2013 IEEE Globecom Workshops (GC Wkshps)*, Atlanta, GA, Dec. 2013, pp. 117–122.

[44] S. Abdallah, M. Saad, K. Alnajjar, and M. Masood, "Semi-blind joint timing-offset and channel estimation for amplify-and-forward two-way relaying," *IEEE Trans. Wireless Commun.*, vol. 19, no. 4, pp. 2613–2627, Apr. 2020.

[45] J. Coon, M. Beach, and J. McGeehan, "Optimal training sequences for channel estimation in cyclic-prefix-based single-carrier systems with transmit diversity," *IEEE Signal Process. Lett.*, vol. 11, no. 9, pp. 719–732, Sep. 2004.

[46] G. H. Golub and C. F. V. Loan, *Matrix Computations*. Baltimore, MD: The Johns Hopkins University Press, 1983.

[47] K. J. Kim, Y. Yue, R. A. Iltis, and J. D. Gibson, "A QRD-M/Kalman Filter-based detection and channel estimation algorithm for MIMO-OFDM systems," *IEEE Trans. Wireless Commun.*, vol. 4, pp. 710–721, Mar. 2005.

[48] A. H. Mehana and A. Nosratinia, "Single-carrier frequency-domain equalizer with multi-antenna transmit diversity," *IEEE Trans. Wireless Commun.*, vol. 12, pp. 388–397, Jan. 2013.

[49] F. Pancaldi, G. M. Vitetta, R. Kalbasi, N. Al-Dhahir, M. Uysal, and H. Mheidat, "Single-carrier frequency domain equalization," *IEEE Signal Process. Mag.*, vol. 25, no. 5, pp. 37–56, 2008.

[50] H. B. Çelebi, A. Pitarokoilis, and M. Skoglund, "Low-latency communication with computational complexity constraints," *2019 16th Int. Symposium on Wireless Commun. Systems (ISWCS)*, pp. 384–388, 2019.

[51] B. Devillers, J. Louveaux, and L. Vandendorpe, "About the diversity in cyclic prefixed single-carrier systems," *Elsevier Physical Communication Journal*, vol. 1, pp. 266–276, Dec. 2008.

[52] T. Yamamoto, K. Takeda, and F. Adachi, "Frequency-domain block signal detection with qrm-mld for training sequence-aided single-carrier transmission," *EURASIP J. Adv. Signal Process.*, vol. 2011, Jan. 2011.

[53] J. N. Laneman and G. W. Wornell, "Energy-efficient antenna sharing and relaying for wireless networks," in *Proc. IEEE Wireless Communications and Networking Conf.*, Chicago, IL, Oct. 2000, pp. 7–12.

[54] K. J. Kim and T. A. Tsiftsis, "On the performance of cyclic prefix-based single-carrier cooperative diversity systems with best relay selection," *IEEE Trans. Wireless Commun.*, vol. 10, no. 4, pp. 1269–1279, Apr. 2011.

[55] K. J. Kim, T. A. Tsiftsis, and G. K. Karagiannidis, "Average rate and outage probability of cyclic prefixed single-carrier opportunistic cooperative diversity systems," in *Proc. 21st Annual IEEE Int'l Symp. on Personal, Indoor and Mobile Radio Commun.*, Instanbul, Turkey, Sep. 2010, pp. 2117–2122.

[56] P. Wu, R. Schober, and V. K. Bhargava, "Robust transceiver design for SC-FDE multi-hop full-duplex decode-and-forward relaying systems," *IEEE Trans. Wireless Commun.*, vol. 15, no. 2, pp. 1129–1145, Feb. 2016.

[57] K. J. Kim, T. Q. Duong, T. A. Tsiftsis, and V. N. Q. Bao, "Cognitive multihop networks in spectrum sharing environment with multiple licensed users," in *Proc. IEEE Int. Conf. Commun.*, Budapest, Hungary, Jun. 2013, pp. 2869–2873.

[58] J.-H. Cui, J. Kong, M. Gerla, and S. Zhou, "The challenges of building mobile underwater wireless networks for aquatic applications," *IEEE Netw.*, vol. 20, no. 3, pp. 12–18, May-Jun. 2006.

[59] F. Li and Y. Wang, "Routing in vehicular ad hoc networks: A survey," *IEEE Veh. Technol. Mag.*, vol. 2, no. 2, pp. 12–22, Jun. 2007.

[60] J. Sydir and R. Taori, "An evolved cellular system architecture incorporating relay stations," *IEEE Commun. Mag.*, vol. 47, no. 6, pp. 115–121, Jun. 2009.

[61] M. Wen *et al.*, "Private 5G networks: Concepts, architectures, and research landscape," *IEEE J. Sel. Topics Signal Process.*, vol. 16, no. 1, pp. 7–25, Jan. 2022.

[62] T. A. Tsiftsis, K. J. Kim, and K. S. Kwak, "Cooperative wireless personal area network systems with partial best relay selection," *Trans. on Emerging Telecommunications Technologies*, vol. 23, no. 2, pp. 133–136, Mar. 2012.

[63] I. Krikidis, J. Thompson, S. Mclaughlin, and N. Goertz, "Amplify-and-forward with partial relay selection," *IEEE Commun. Lett.*, vol. 12, no. 4, pp. 235–237, Apr. 2008.

[64] D. Chen, S. Yin, Q. Zhang, M. Liu, and S. Li, "Mining spectrum usage data: A large-scale spectrum measurement study," in *Proc. Int. Conf. Mobile Computing and Networking*, Beijing, China, Sep. 2009, pp. 13–24.

[65] J. Mitola and G. Q. Maguire, "Cognitive radios: Making software radios more personal," *IEEE Personal Commun. Mag.*, vol. 6, pp. 13–18, Aug. 1999.

[66] R. Etkin, A. Parekh, and D. Tse, "Spectrum sharing for unlicensed bands," *IEEE J. Sel. Areas Commun.*, vol. 25, no. 3, pp. 517–528, Apr. 2007.

[67] S. Haykin, "Cognitive radio: Brain-empowered wireless communications," *IEEE J. Sel. Areas Commun.*, vol. 23, no. 2, pp. 201–220, Feb. 2005.

[68] A. Ghasemi and E. S. Sousa, "Fundamental limits of spectrum-sharing in fading environments," *IEEE Trans. Wireless Commun.*, vol. 6, no. 2, pp. 649–658, Feb. 2007.

[69] K. J. Kim, T. Q. Duong, and X. Tran, "Performance analysis of cognitive spectrum-sharing single-carrier systems with relay selection," *IEEE Trans. Signal Process.*, vol. 60, no. 12, pp. 6435–6449, Dec. 2012.

[70] J. Guo, S. Durrani, and X. Zhou, "Performance analysis of arbitrarily-shaped underlay cognitive networks: Effects of secondary user activity protocols," *IEEE Trans. Commun.*, vol. 63, no. 2, pp. 376–389, Feb. 2015.

[71] A. Ghasemi and E. S. Sousa, "Interference aggregation in spectrum-sensing cognitive wireless networks," *IEEE J. Sel. Topics Signal Process.*, vol. 2, no. 1, pp. 41–56, Feb. 2008.

[72] S. Lin *et al.*, "Advanced dynamic channel access strategy in spectrum sharing 5G systems," *IEEE Wireless Commun.*, vol. 24, no. 5, pp. 74–80, Oct. 2017.

[73] K. Chang, "IEEE 802 standards for TV white space," *IEEE Wireless Commun.*, vol. 21, no. 2, pp. 4–5, Apr. 2014.

[74] A. Mirdamadi and M. Sabbaghian, "Spectrum sensing of interleaved SC-FDMA signals in cognitive radio networks," *IEEE Trans. Veh. Technol.*, vol. 64, no. 4, pp. 1633–1637, Apr. 2015.

[75] Y.-C. Liang, Y. Zeng, E. Peh, and A. T. Hoang, "Sensing-throughput tradeoff for cognitive radio networks," *IEEE Trans. Wireless Commun.*, vol. 7, no. 4, pp. 1326–1337, Apr. 2008.

[76] V. M. Blagojevic and P. N. Ivanis, "Ergodic capacity of spectrum sharing cognitive radio with MRC diversity and Nakagami fading," in *Proc. IEEE Wireless Commun. and Netw. Conf.*, Paris, France, Apr. 2012, pp. 2797–2801.

[77] H. V. Poor and R. F. Schaefer, "Wireless physical layer security," *Proc. Nat. Acad. Sci. USA*, vol. 114, pp. 19–26, Jan. 2017.

[78] N. Yang *et al.*, "Artificial noise: Transmission optimization in multi-input single-output wiretap channels," *IEEE Trans. Commun.*, vol. 63, no. 5, pp. 1771–1783, May 2015.

[79] H.-M. Wang, Q. Yin, and X.-G. Xia, "Distributed beamforming for physical-layer security of two-way relay networks," *IEEE Trans. Signal Process.*, vol. 60, no. 7, pp. 3532–3545, Jul. 2012.

[80] L. Dong, Z. Han, A. P. Petropulu, and H. V. Poor, "Improving wireless physical layer security via cooperative relays," *IEEE Trans. Signal Process.*, vol. 58, no. 3, pp. 1875–1888, Mar. 2010.

[81] K. J. Kim, H. Liu, M. Wen, P. Orlik, and H. V. Poor, "Secrecy performance analysis of distributed asynchronous cyclic delay diversity-based cooperative single carrier systems," *IEEE Trans. Commun.*, vol. 68, no. 5, pp. 2680–2694, May 2020.

[82] K. J. Kim, M. D. Renzo, H. Liu, T. A. Tsiftsis, P. V. Orlik, and H. V. Poor, "Distributed cyclic delay diversity systems with spatially distributed interferers," *IEEE Trans. Wireless Commun.*, vol. 18, no. 4, pp. 2066–2079, Jun. 2019.

[83] Q. Li, Q. Yan, K. C. Keh, K. H. Li, and Y. Hu, "A multi-relay-selection scheme with cyclic delay diversity," *IEEE Commun. Lett.*, vol. 17, no. 2, pp. 349–352, Feb. 2013.

[84] K. J. Kim, H. Liu, M. D. Renzo, and H. V. Poor, "Performance analysis of spectrum sharing systems with distributed CDD," in *Proc. 2018 IEEE GLOBECOM*, Abu Dhabi, United Arab Emirates, 4-8 Dec. 2018, pp. 206–212.

[85] N. Iradukunda, H. T. Nguyen, and W. Hwang, "On cyclic delay diversity-based single-carrier scheme in spectrum sharing systems," *IEEE Commun. Lett.*, vol. 23, no. 6, pp. 1069–1072, Jun. 2019.

[86] W. Zhang, C. Wang, X. Ge, and Y. Chen, "Enhanced 5G cognitive radio networks based on spectrum sharing and spectrum aggregation," *IEEE Trans. Commun.*, vol. 66, no. 12, pp. 6304–6316, Dec. 2018.

[87] M. Norin *et al.*, "5G spectrum for local industrial networks," *Ericsson White Paper*, pp. 1–25, 2020.

[88] K. J. Kim *et al.*, "A dCDD-based transmit diversity scheme for downlink pseudo-NOMA systems," *IEEE Trans. Wireless Commun.*, vol. 20, no. 2, pp. 1217–1232, Feb. 2021.

[89] ——, "A multi-cluster-based distributed CDD scheme for asynchronous joint transmissions in local and private wireless networks," *IEEE Trans. Wireless Commun.*, vol. 21, no. 1, pp. 80–94, Jan. 2022.

[90] Qualcomm, "How CoMP can extend 5G NR to high capacity and how comp can extend 5G NR high capacity and ultra-reliable communications," accessed: June 22, 2021.